Characterization of Real Fractal Objects

Analysis of the Box Counting Approach with Applications to Gas-Evaporated Metal Aggregates

Jan R. M. Röman

Department of Applied Physics
Chalmers University of Technology and Göteborg University
Göteborg Sweden

Uppsats för avläggande av teknisk licentiatexamen i teoretisk fysik vid Chalmers tekniska högskola.
Uppsatsen presenteras vid ett seminarium fredagen den 6:e oktober 1995 kl. 13.15 i Forskarhuset Fysik, Chalmers tekniska högskola, sal F6217

Uppsatsen finns tillgänglig vid institutionen för tillämpad fysik

This thesis consists of an introduction and the following papers:

I. FINITE-SIZE EFFECTS ON THE CHARACTERIZATION OF FRACTAL SETS : f(α) CONSTRUCTION VIA BOX COUNTING ON A FINITE TWO-SCALED CANTOR SET.
J. Håkansson* and G. Russberg
Phys. Rev. A**41**, 1855 (1990).

II. FINITE-SIZE EFFECTS ON THE CHARACTERIZATION OF FRACTAL SETS II: f(α) CONSTRUCTION VIA BOX COUNTING ON A FINITE TWO-SCALED SNOWFLAKE FRACTAL.
J. Håkansson*
NORDITA Preprint-89/60 S.

I. MULTIFRACTAL ANALYSIS OF GAS EVAPORATED METAL PARTICLE AGGREGATES.
J. Håkansson* * and G. A. Niklasson
Z. Physik D**20**, 317 (1991).

* Jan Håkansson has changed family name and is now Jan R. M. Röman

Acknowledgements

This work has been supported by the Swedish Natural Science Research Council, which is gratefully acknowledged. I also would like to thank my supervisor Prof. Stig Lundqvist for introducing me to the field of dynamical systems. chaos and fractals. My other supervisors Prof. Mats Jonson and Dr. Predrag Cvitanovic, is gratefully acknowledged for all their advice and discussions that came up under this work. I also want to thank Dr. Gunnar Nicklasson for introducing me to fractal aggregate and practical use of fractals and Dr. Gunnar Russberg for his valuable comments on this manuscript. Finally, I want to thank all my colleagues at Chalmers and NORDITA in Copenhagen.

1. INTRODUCTION

One question one may ask about fractals is: Why do we need non-integer dimensions? A short answer to the question is that for some strange objects it is not possible to find a well defined measure (other than zero) without introducing non-integer or fractal dimensions. What this means will be explained later in the thesis.

A fractal object in three dimensional space is characterized by a large surface-to-volume ratio. For example, the need of a rapid gas exchange explains the existence of the large surface-to-volume ratio observed in a lung. The area of a human lung measured with the resolution 100 μm is as large as that of a tennis-court (has the size of 10^2 m^2) while the volume enclosed by it is a few litres [1] (has the size of 10^{-3} m^3). Another case where a large surface-to-volume ratio is needed, is for the materials used for efficient catalysis. A characteristic property of a fractal is that its measure depends on the resolution used in the measurement. Typically, the surface area of an object converges very fast to a finite limiting value as the resolution is increased, but for fractals the area diverges

The theory of fractals radically differs from traditional Euclidean geometry, fractal geometry describes objects that are self-similar, or scale invariant. This means that when some parts of such an object is magnified; it is seen to bear an exact resemblance to the whole, the likeness continuing with the parts of the parts and so on to infinity. The self-similar structure is perhaps the main reason for the striking beauty of so many fractals [2]. A set is strictly self-similar if it can be expressed as a union of sets, each of which is a reduced copy of (is geometrically similar to) the full set. However, not all fractal objects exhibit this precise form. In a coastline, for instance, there is an irregular nesting of gulfs, bays, harbours, and coves that are observed over a broad range of spatial scales. A magnified view of one part of the coastline

may not precisely reproduce the full picture, but it will have the same qualitative appearance. A coastline displays the kind of fractal behaviour that is called statistical self-similarity. Fractals also must be devoid of translational symmetry--that is, the smoothness associated with Euclidean lines, planes, and spheres. Instead a rough, jagged quality is maintained at every scale at which an object can be examined. The nature of fractals is reflected in the word itself, coined by Benoit B. Mandelbrot, [3] derived from the Latin verb frangere, "to break," and the related adjective fractus, "irregular and fragmented." His book "*The Fractal Geometry of Nature (1982)*" is the standard reference and contains both the elementary concepts and an unusually broad range of new and rather advanced ideas, such as multifractals, currently under active study.

The simplest fractal is the Cantor bar (named after the 19th- century German mathematician Georg Cantor). It is constructed by dividing a line in 3 intervals and removing the middle interval. The procedure is repeated indefinitely, first on the 2 remaining intervals, then on 4 intervals produced by that operation, and so on, until the object has an infinitely large number of intervals each of which is infinitely small.

Fractals are not relegated exclusively to the realm of mathematics. If the definition is broadened a bit, such objects can be found virtually everywhere in the natural world. The difference is that "natural" fractals are randomly, statistically, or stochastically rather than exactly scale symmetric. The rough shape revealed on one length scale bears only an approximate resemblance to that on another, but the length scale being used is not apparent just by looking at the shape. Moreover, there are both upper and lower limits to the range in size over which the fractals in nature are indeed fractal. Above and below that range, the shapes are either rough (but not self-similar) or smooth--in other words, conventionally Euclidean.

Whether natural or mathematical, all fractals have particular fractal dimensions. These are not the familiar Euclidean dimensions given by integers--1, 2, or 3--but a different kind of quantity. Usually noninteger, a fractal dimension indicates the extent to which the fractal object fills the Euclidean dimension in which it is embedded. A natural fractal of fractal dimension 2.8, for example, would be a sponge-like shape nearly 3-dimensional in appearance. A natural fractal of fractal dimension 2.2 would be a much smoother object that just misses being flat.

The roots of fractal geometry can be traced to the late 19th century, when mathematicians started to challenge Euclid's principles. Fractional dimensions were not discussed until 1919, however, when the German mathematician Felix Hausdorff[4] put forward the idea in connection with the small-scale structure of mathematical shapes. As completed by the Russian mathematician A. S. Besicovitch, Hausdorff's dimensionality was a

forerunner of fractal dimensionality. Other mathematicians of the time, however, considered such strange shapes as "pathologies" that had no significance.

This attitude persisted until the mid-20th century and the work of Mandelbrot. His 1961 study of similarities in large- and small-scale fluctuations of the stock market was followed by work on phenomena involving nonstandard scaling, including the turbulent motion of fluids and the distribution of galaxies in the universe. A 1967 paper on the length of the English coast showed that irregular shorelines are fractals whose lengths increase with increasing degree of measurable detail. By 1975, Mandelbrot had developed a theory of fractals, and publications by him and others made fractal geometry accessible to a wider audience. The subject began to gain importance in the sciences. As mentioned, fractal geometry appears in many fields of science, in the study of landscapes (e.g., coast lines, mountains, rivers and sediments), in the study of plants, metals and composite materials, in crystals, aggregates, flows, galaxy formations, populations and in economical systems etc. The dimensions and scaling indices also characterise universality classes of systems. They are equal for systems of a given class, since they describe the same scaling properties.

Mandelbrot later also investigated another fractal terrain, that of shapes distorted in some way from one length to another. These fractals are now called nonlinear, since the relationships between their parts is subject to change. They retain some degree of self-similarity, but it is a local rather than global characteristic in them. The general definition of the word fractal may thus need further refinement, to indicate more precisely which shapes should be included and which excluded by the term.

The most intriguing of the nonlinear fractals thus far has been the mathematical set named after Mandelbrot by the American mathematicians John Hubbard and Adrien Douady. The more the set is magnified, the more its unpredictability increases, until unpredictability comes to dominate the bud-like shape that is the set's major element of stability. The set has become the source of stunning colour computer graphics images. It is also important in mathematics because of its centrality to dynamical system theory. An entire Mandelbrot set is actually a catalogue of dynamical mathematical objects--that is, objects generated through an iterative process called Julia sets. These derive from the work done by a French mathematician, Gaston Julia, on the iteration of nonlinear transformations in a complex plane.

Scientists have begun to investigate the fractal character of a wide range of phenomena[5], [6]. Researchers are interested in doing so for the practical reason that behaviour on a fractal shape may differ markedly from that on a Euclidean shape. Physics is by far the discipline most affected by fractal geometry. In condensed-matter, or solid-state physics, for example, the so-

called "percolation cluster" model used to describe critical phenomena involved in phase transitions and in mixtures of atoms with opposing properties is clearly fractal. This has implications, as well, for a host of attributes, including electrical conductivity. The percolation cluster model may also apply to the atomic structure of glasses, gels, and other amorphous materials, and their fractal nature may give them unique heat-transport properties that could be exploited technologically.

Mathematical physics, for its part, has a particular interest in nonlinear fractals. When dynamical systems--those that change their behaviour over time--become chaotic, or totally unpredictable, physicists describe the route they take with such fractals. Called strange attractors, these objects are not real physical entities but abstractions that exist in "phase space," an expanse with as many dimensions as physicists need to describe dynamical physical behaviour. One point in phase space represents a single measurement of the state of a dynamical system as it evolves over time. When all such points are connected, they form a trajectory that lies on the surface of a strange attractor. Most physicists who study chaos do so with carefully controlled laboratory setups of turbulent fluid flow. Individual strange attractors have been identified for different kinds of turbulent fluid flow, suggesting the existence of numerous routes to chaos [7], [8], [9].

Although not concerned with fractals to the same extent as physics, other sciences have discovered them. In biology, the anomolous thermal relaxation rate of iron-containing proteins has been explained as resulting from the fractal shape of the linear polymer chain that comprises all proteins. The distribution pattern of atoms on the protein surface, a different aspect of protein structure, also appears to be fractal. Many more fractals have been detected in geology, including both random exterior surfaces--ragged mountains and valleys--and interior fractal surfaces in the brittle crust, such as California's famous San Andreas fault. Earthquake processes for small tremors--those of magnitude 6 or less--appear to be fractal in time as well as space, since these quakes occur in self-similar clusters rather than at regular intervals. Meteorology provides a different kind of space-time fractal: the contour of the area over which tropical rain falls is self-similar, and the amount of rain that falls varies in a self-similar fashion over time. Finally, on the interface of science and art, computer-graphics specialists, using a recursive splitting technique, have produced striking new fractal images of great statistical complexity. Landscapes made this way have been used as backgrounds in many motion pictures; trees and other branching structures have been used in still lifes and animations.

Another major area of condensed-matter physics to invoke the concept of self-similarity is that of kinetic growth, in which particles are gradually added to a structure in such a way that once they stick, they neither come off

nor rearrange themselves. In the case of the simplest model of kinetic growth, the most important physical phenomenon to which it applies appears to be the fingering of a less-viscous fluid (water) through a more viscous fluid (oil) lodged in a porous substance (limestone and other kinds of rock). A more complex model explains the growth of colloidal agglomerates.

FRACTAL DIMENSION

Fractal dimension can be defined in many ways, but before giving a definition I would like to discuss how to measure the size of general (fractal) objects. Since we want to measure objects with varying degree of resolution, we cover them by boxes, squares or line-segments and count how many are needed for a complete covering. In the following we will call squares and line-segments boxes (in two and one dimension respectively) as well. The objects are covered/enclosed in d-dimensional boxes of size l, where d is the topological dimension of the set. The topological dimension is always an integer. The fractals we will discuss may be considered to be sets of points in coordinate space or in phase-space. They may be single isolated points like galaxies in the Universe or molecules combined to complicated patterns like aggregates. The set of points that make up a line in Euclidean space has the topological dimension $d = 1$, and the fractal dimension $D = 1$. The set of points that form a sheet has $d = 2$, $D = 2$ and a ball $d = 3$ and $D = 3$.

2.1: Measuring general sets

To illustrate the general method of measuring, consider a smooth curve in Euclidean space, see *Fig. 1*.

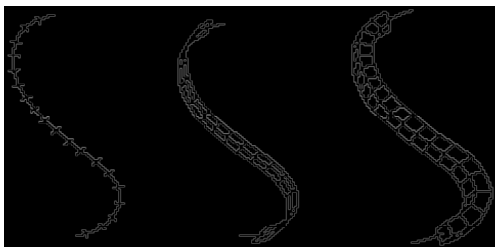

Figure 1. The total measure (length, area and volume) of the curve is found by counting the number of boxes needed for the covering, multiplied with the box-size (l, l^2, l^3) in the limit $l \to 0$.

The measure (here the length) of the curve is found by counting the number of equally sized line-segments of length l, $N(l)$, needed to cover the curve. The total length is then given by

$$L = \lim_{l \to 0} N(l) \cdot l = L_0 l^{-1} l^1 = L_0 l^0 = L_0 \qquad (1)$$

since the number of segments needed to cover the curve is inversely proportional to the segment size, i.e., $N(l) \propto l^{-1} = L_0 l^{-1}$. In the limit $l \to 0$ the measure asymptotically equals the length of the curve and is independent of l. If we instead measure the area of the curve we replace the line-segments by a grid of squares. The total area of the curve is then given by

$$A = \lim_{l \to 0} N(l) \cdot l^2 = A_0 l^{-1} l^2 = A_0 l^1 = 0 \qquad (2)$$

Similarly the volume of the curve is zero. We observe that the only interesting measure of a curve is the length, i.e., the only meaningful dimension of a curve is $d = 1$.

If we instead consider a set of points defining a smooth surface in Euclidean space, we cover the set with squares of size l^2 and counts the number of squares needed to cover the set, see *Fig. 2*.

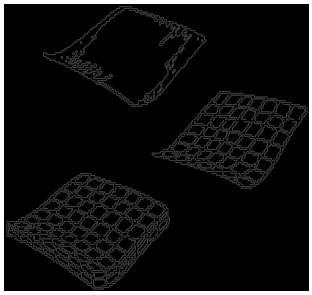

Figure 2. The total measure (length, area and volume) of a surface is found by counting the number of boxes needed for the covering, multiplied with the box-size (l, l^2, l^3) as $l \to 0$.

The measure of the area is then given by

$$A = \lim_{l \to 0} N(l) \cdot l^2 = A_0 l^{-2} l^2 = A_0 l^0 = A_0 \qquad (3)$$

where N(l) $\propto l^{-2} = A_0 l^{-2}$. Similarly we can define a "length" and a "volume" of the surface by

$$L = \lim_{l \to 0} N(l) \cdot l = L_0 l^{-2} l^1 = L_0 l^{-1} = \infty \qquad (4)$$

and

$$V = \lim_{l \to 0} N(l) \cdot l^3 = V_0 l^{-2} l^3 = V_0 l^1 = 0 \qquad (5)$$

As we can see, the only interesting measure of a surface is the area. In other words; the only interesting dimension for the study of an ordinary smooth surface in Euclidean space is $d = 2$. However, one may easily define sets of points that are curves, which twist so badly that their length is infinite (see the triadic Koch curve below, in the limit $n \to \infty$). Some curves, so called Peano curves even fill the plane. Before discussing such strange sets we have to generalize the measure of size for a given set.

In general, the d-dimensional measure is defined as

$$M_d = \lim_{l \to 0} N(l) \cdot l^d \qquad (6)$$

where $N(l)$ is the number of boxes of size l needed to cover the curve and d the topological dimension of the set. As $l \to 0$, three things may happen. 1) If $d > D$, the measure diverges; 2) if $d < D$, the measure becomes zero. Only when 3) $d = D$ the measure may approach a finite, non zero value. Thus, by requiring M_d to be constant (not zero), we define the value of the critical dimension D which we will refer to as the fractal dimension. In the literature there exist alternative definitions of fractal dimension [3-6]. The important property in the calculation of fractal dimensions is how the number of boxes needed to cover the set scales with the box-size. This means that if $N(l) \propto l^{-D}$ in the limit $l \to 0$, only $d = D$ gives a finite measure since

$$M_d = \lim_{l \to 0} N(l) \cdot l^d \propto \lim_{l \to 0} l^{d-D} = const. \qquad (7)$$

We may therefore determine the fractal dimension of an object from the slope of *ln N(l)* plotted as a function of *ln l* (see e.g. *Fig. 5*). An object will be called fractal if its observed measure depends on the resolution (box-size) over several orders of magnitude, and follows a power law behaviour with a nontrivial exponent. This dependence can be observed over an infinite range of the resolution in the case of fractals generated by mathematical constructions. Such fractals have no smallest and no largest scale. In contrast, fractals used to model growth processes like aggregation of magnetic particles (see paper III) have a smallest scale due to a finite particle size. However, such fractals can be made from a mathematical construction. This can be made by halting the iteration at a finite level as the snowflake fractal in paper II. In real physical systems, there also exists a lower cut-off for the box-size since the fractal structure is replaced by different patterns when approaching the microscopic scales. Therefore a straight line in the plot of *ln N(l)* vs. *ln l* can be observed only in some range of *l*. This range must extend over several decades in order to imply the existence of a fractal structure.

2.2: A one-scaled Cantor set (part 1)

A very simple method to construct fractal sets with a fractal dimension in the range $0 < D < 1$ is shown in *Fig. 3*.

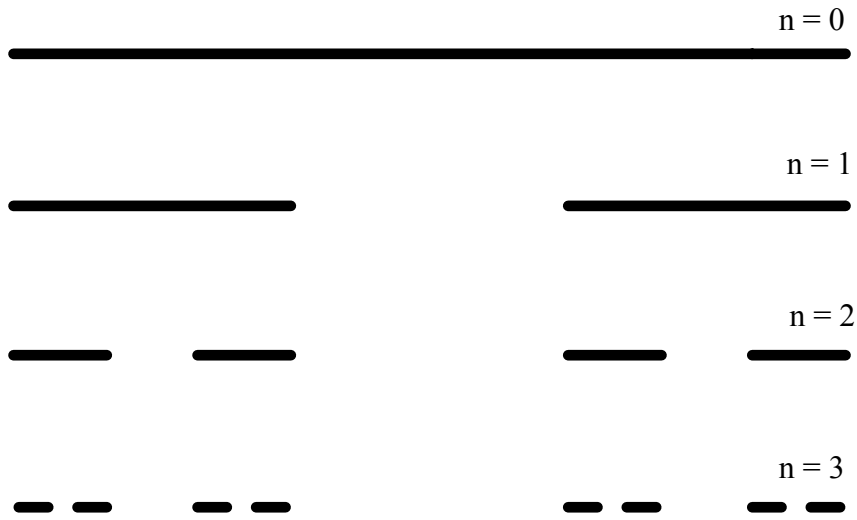

Figure 3. The first three steps in the construction of a one-scaled Cantor set. At each stage of construction the central third of each segment is removed from the set. For the resulting fractal D = 0.631...

One starts out with a unit interval [0,1] and replaces it by N smaller intervals. In the example a unit interval is replaced by two new intervals of length $1/3$. By repeating the procedure on each of the remaining intervals ad infinitum one gets a set of remaining points called a one-scaled Cantor set. The simple construction of the set makes it easy to calculate the fractal dimension, since we know the number of intervals (boxes) on any level of construction. Let us use a grid obtained by dividing the unit interval into 3^n equal intervals (n is a fixed integer). As follows from the construction, the number of such pieces (of size 3^{-n}) needed to cover the Cantor set is 2^n.

We then have $l = 3^{-n}$ and $N(l) = 2^n$ which gives

$$M_d = \lim_{l \to 0} N(l) \cdot l^d \propto \lim_{l \to 0} 2^n \cdot 3^{-d \cdot n} \qquad (8)$$

This measure diverges or approaches zero, unless we choose $d = D = \ln 2/\ln 3 = 0.6309...$ From the generalised measure we can then define the fractal dimension as

$$D = \lim_{n \to \infty} \frac{\ln N(l)}{\ln(1/l)} \tag{9}$$

Since the Cantor set is given by a mathematical construction (a recursive rule) the scaling behaviour exist over an infinite range of resolution. A fractal as the Cantor set is called a *deterministic fractal* since it can be constructed by a deterministic rule. The Cantor set is also a *self-similar* object. Such objects can be divided into N identical parts, each being a rescaled version, by a factor r, of the complete set. Let $N_1(l)$ denote the number of boxes on a grid of size $l << L$ (L is the size of the fractal) needed to cover one such part. The number of boxes needed to cover the complete fractal is then

$$N(l) = N \cdot N_1(l) \tag{10}$$

Due to the self similarity, $N_1(l)$ equals the number of boxes needed to cover the complete set with boxes of size l/r, i.e.,

$$N_1(l) = N(1/r) \tag{11}$$

The fractal dimension is then given by

$$D = \frac{\ln N}{\ln(1/r)} \tag{12}$$

which is an exact result for one-scaled fractals [3].

2.3: Coast lines and the triadic Koch curve

A common example of fractal objects is coastlines. The length of a coastline depends critically on the length of the yardstick used to measure the distance between points along the coast. Smaller yardstick gives a larger measure of the coast.

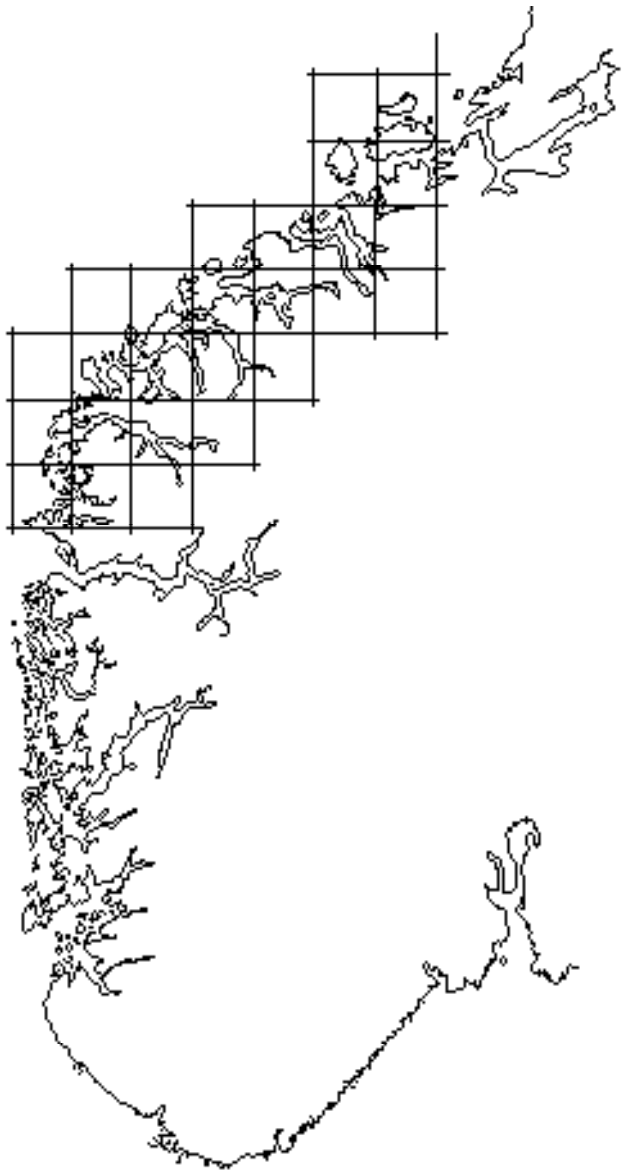

Figure 4. The coast of the southern part of Norway. The outline was traced from an atlas and digitized at about 1800 x 1200 pixels [12]. The shown grids has a size l ~ 50 km.

Fig. 5 shows how the measured length increases as the yardstick length, *l*, is reduced. This *log-log* plot shows that the measured coastline shows no sign to reaching a fixed value as *l* is reduced. In fact, the measured length is nicely approximated by the formula

$$L(l) = a \cdot l^{1-D}. \qquad (13)$$

If we suppose the coast to have a well defined length L_N we would expect it to be L_N, at least for small enough *l*, and the exponent should be

equal to one. However, for the coastline of Norway, see *Fig. 4* the value of *D* is found to be *1.52* [12].

In *Fig. 6* we show a reproduction of the data collected by Richardson (from Mandelbrot's (1982) book [3]) showing the apparent length of various coastlines and boundaries. They all fall on straight lines in the *log-log* plot except for the circle for which the measure converge to a finite value.

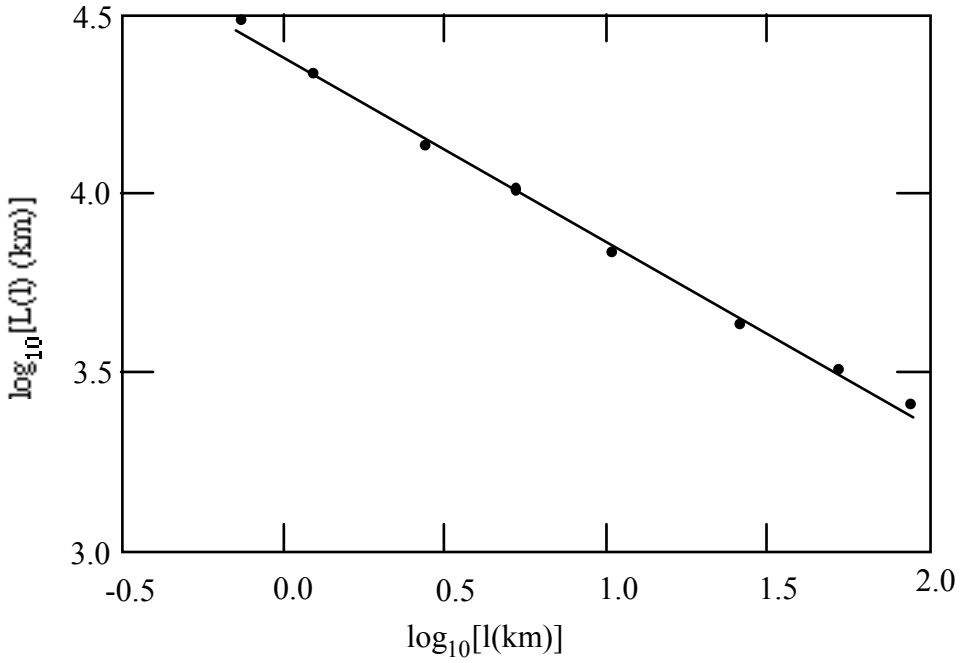

Figure 5. The measured length of the coast of Norway as function of the yardstick l. The straight line in this log-log plot corresponds to the relation $L(l) = a \cdot l^{1-D}$, *with* $D \approx 1.52$.

The slope of the lines in the plot is *1 - D*, where *D* is the fractal dimension of the coastline. As model for such a coastline we will study a simple set called the triadic Koch curve, (see *Fig. 7*). The set is constructed from a unit interval, which we call the *0-th* generation of the Koch curve.

By replacing this interval by the polygon marked $n = 1$ we get the first generation of the set. If we then continue and replace each of the four segments with a new polygon and so on, we get in the limit $n \to \infty$ a fractal set. Since the set is generated by the polygon marked $n = 1$ this polygon is called the *generator* of the Koch curve.

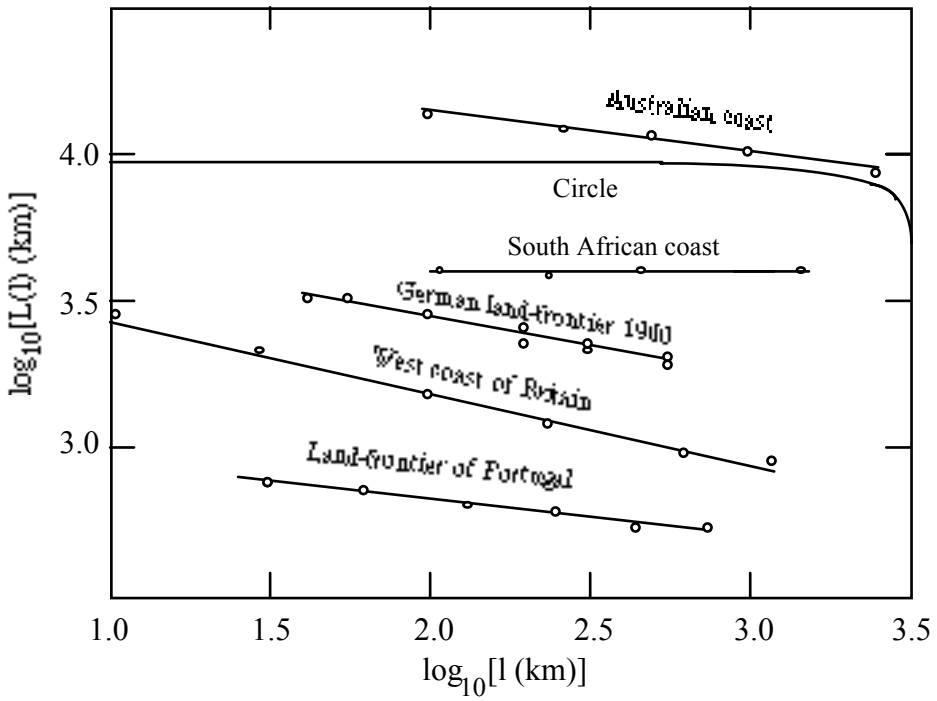

Figure 6. The length of coastlines as a function of the yardstick length (Mandelbrot, 1982).

The Koch curve have in the limit $n \to \infty$ an infinite length, an area $A = 0$, and therefore not a well defined measure in an integer dimension. At a given level n the curve consists of 4^n segments, each of length 3^{-n}. We then find the fractal dimension of the Koch curve to be

$$D = \lim_{n \to \infty} \frac{\ln 4^n}{\ln 3^n} = \frac{\ln 4}{\ln 3} \qquad (14)$$

The topological dimension of the set must be equal to one since we can stretch the curve to a straight line after each step in the construction. We then conclude that the Koch curve is a fractal set with dimension
$D = ln\ 4/ln\ 3$.

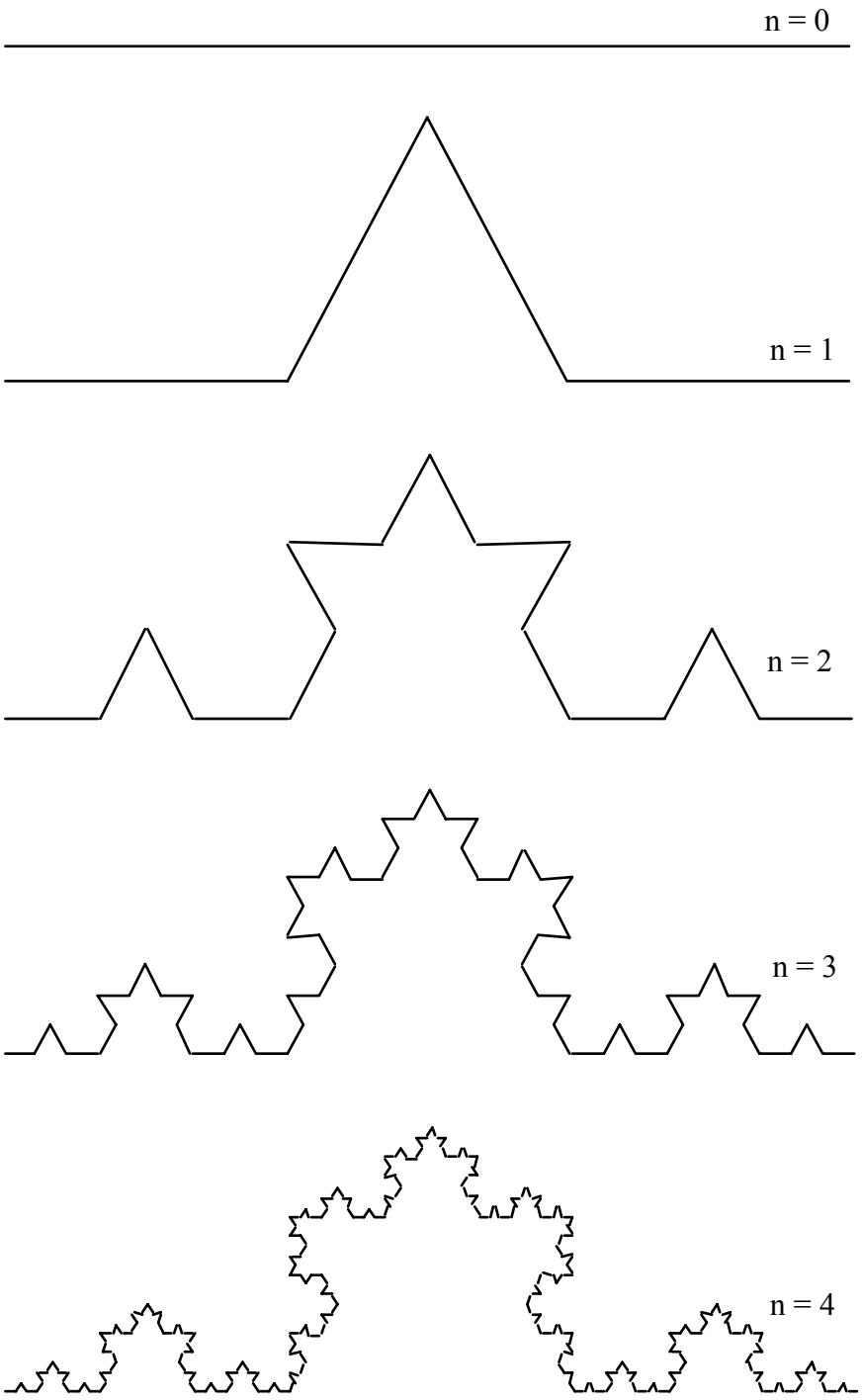

Figure 7. The construction of the triadic Koch curve. By replacing each line segment with a resized copy of the part marked n = 1 we construct a fractal with D = ln 4/ln3.

2.4: Some simple fractals in d = 2

In two dimensions it is easy to construct fractal sets by instead of using an interval, using a square and removing parts of it recursively. First we

prove that we can construct a one-dimensional set by partitioning a unit square into nine new squares and removing six of them as shown in *Fig. 8*. Repeating the procedure with the three remaining squares ad infinitum, we end up with a straight line. The size of the squares at level n is $(1/3)^n$ and the number of squares of that size needed to cover the set is 3^n. We get $D = 1$ just as we can expect. Since the topological dimension $d = 1$, the remaining set is not a fractal.

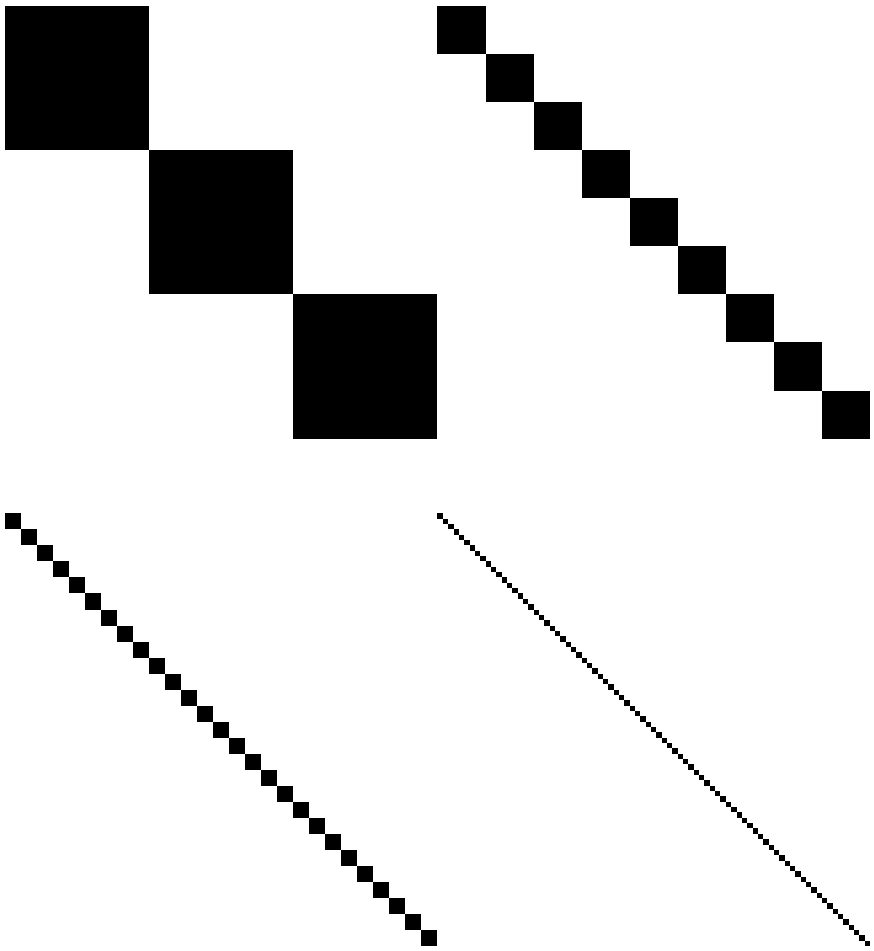

Figure 8. The construction of a "fractal" set with D = 1.

If we instead construct a snowflake by dividing a square into nine parts and remove four of them (see *Fig. 9*) we get in the limit $l \to 0$ (<=> $n \to \infty$) 5^n squares of size $(1/3)^n$ and then $D = (\ln 5)/(\ln 3)$.

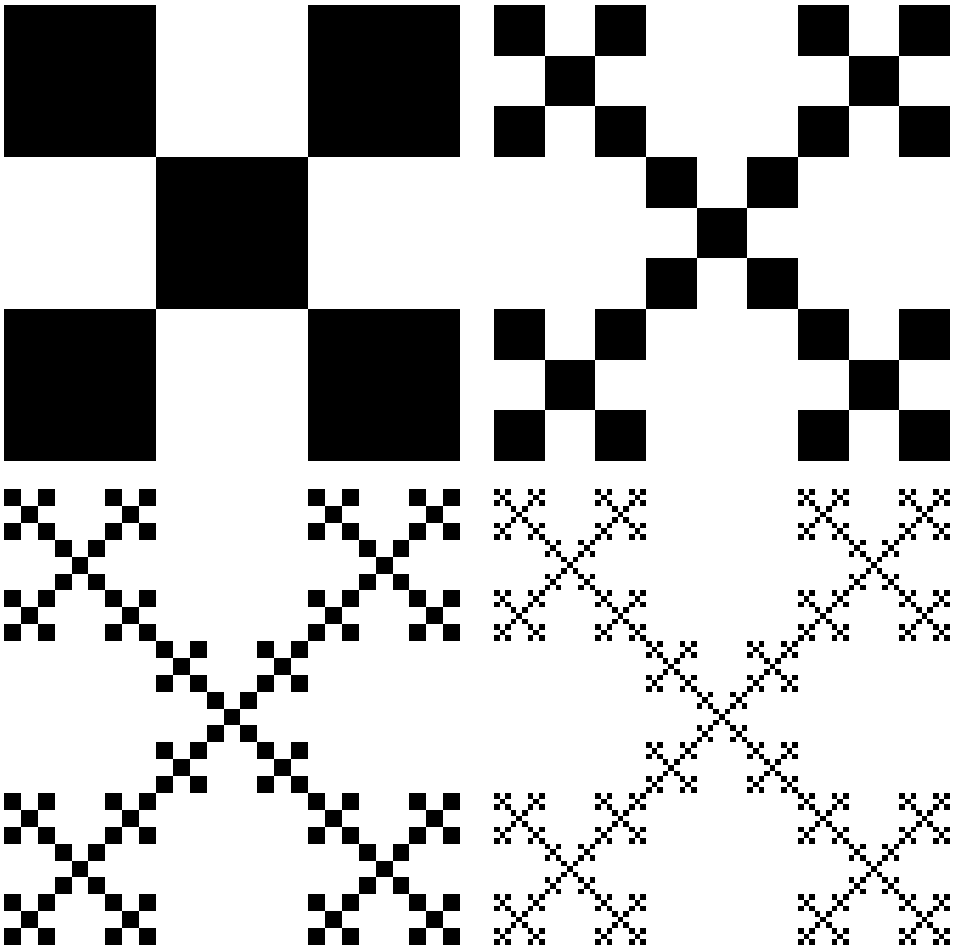

Figure 9. A one-scaled snowflake fractal.

We observe that if we remove six squares we get $D = 1$. It is possible to generate different fractal sets with the same fractal dimension. This is illustrated in *Fig. 10* and *Fig. 11* where we have divided two squares in nine pieces and removed five of them recursively. Both have the fractal dimension $D = \ln 4/\ln 5$.

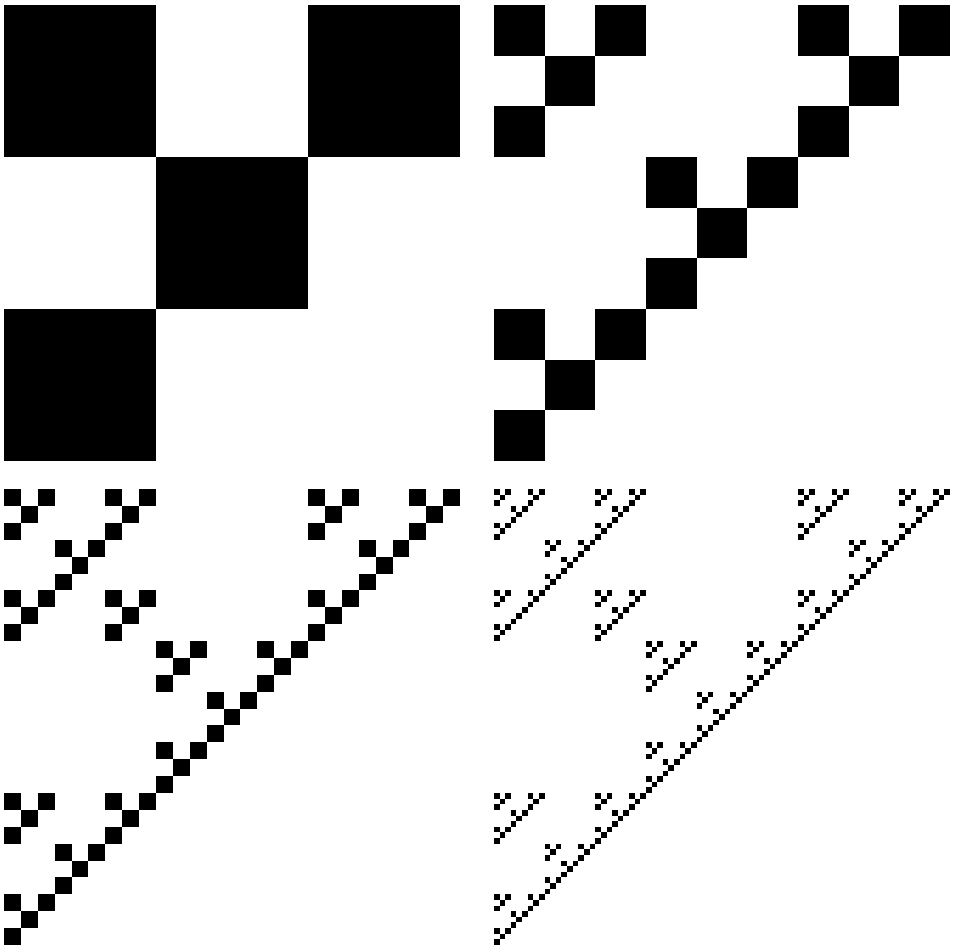

Figure 10. A fractal measure of dimension D = ln 4/ln 5. Compare this fractal with Fig 11. which has the same fractal dimension.

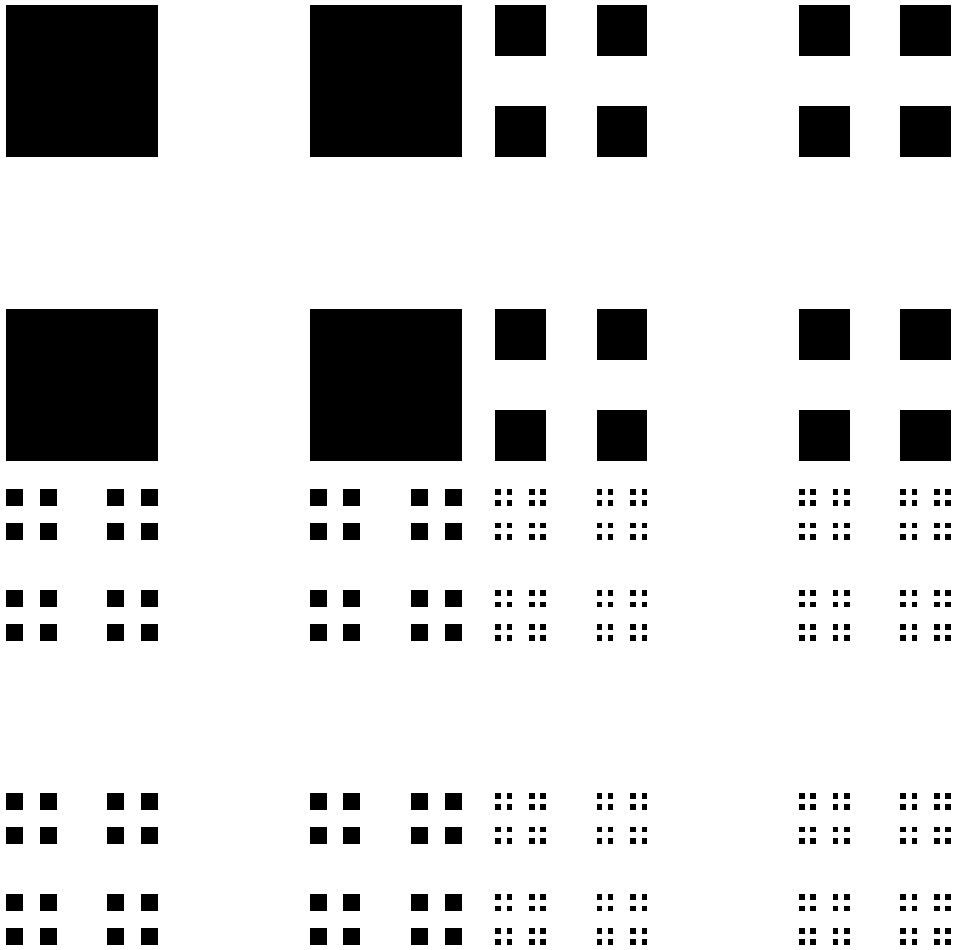

Figure 11. A second fractal measure of dimension D = ln 4/ln 5. Compare this set with the set in Fig 10.

3. MULTIFRACTALS

We have so far only studied objects that are fully characterized by a single value *D*, the *Hausdorff dimension*, hence forth denoted by D_0. Fractals found in nature however, most often need for their characterisation a whole spectrum of dimensions called *generalized dimensions* D_q. The Hausdorff dimension is only one dimension in this continuous spectrum. Such fractals are called multifractals. The essential difference between the construction of multifractals and (one-scaled) fractals is that the initial set is divided into *N* not identically sized parts. Each sub-set is a reduced version of the original object by some factor. The procedure is repeated self-similarly ad infinitum.

A starting point in the study of multifractal objects is the construction of a partition function Γ [13]. The set is covered with a grid of boxes numbered *i = 1, 2, ..., N* of (for simplicity of equal) size *l*. *N = N(l)* is the total number of boxes of size *l* needed to cover the set. The probability to find some part of the fractal in box *i*, p_i, is then equal to the number of points in the box *(= n_i)* divided by the total number of points in the complete set, i.e., the total normalized mass, $M = \sum n_i$. The partition function is then given by

$$\Gamma(\tau, q) = \sum_{i=1}^{N(l)} \frac{(p_i)^q}{l_i^{\tau}} = \frac{1}{M^q} \sum_{i=1}^{N(l)} \frac{(n_i)^q}{l_i^{\tau}} = \frac{1}{l^{\tau} \cdot M^q} \sum_{i=1}^{N(l)} (n_i)^q \qquad (15)$$

where τ is called the *mass exponent* ,*q* the *moment order* and l_i is the length of the *i´*th box. In Eq. (15) we assume that all lengths l_i have the same size *l*.

Depending on τ and *q* three things may happen in the calculation of Γ. If for fixed *q*, τ is greater than some τ(*q*) the partition sum diverges to infinity. On the other hand, if τ is less than τ(*q*) the sum converges to zero. Only if τ is exactly equal to τ(*q*) the sum approaches a finite value different from zero

$$\lim_{\max\{l_i\} \to 0} \Gamma(\tau, q, \{l_i\}) = \begin{cases} \infty & if \quad \tau > \tau(q) \\ const. & if \quad \tau = \tau(q). \\ 0 & if \quad \tau < \tau(q) \end{cases} \qquad (16)$$

Compare this with the discussion of general measure in section 2.1, Eq. (7). Thus, by requiring Γ = constant (not zero) we define the relationship between τ and *q*. If we normalize the probabilities p_i i.e., $\sum p_i = 1$, give Γ = 1. The function τ(*q*), sometimes called the *free energy*, is then given by

$$\tau(q) = \lim_{l \to 0} \frac{1}{\ln l} \cdot \ln\left(\sum_{i=1}^{N(l)} (p_i)^q \right) \qquad (17)$$

We then define the generalized dimensions D_q [14 - 17] as

$$(q-1) D_q = \tau(q) \qquad (18)$$

i.e.,

$$D_q = \lim_{l \to 0} \frac{1}{(q-1)\ln l} \cdot \ln\left(\sum_{i=1}^{N(l)} (p_i)^q \right) \qquad (19)$$

If we put *q = 0* we get the original expression for the Hausdorff dimension

$$D_0 = \lim_{l \to 0} \frac{\ln N(l)}{\ln(1/l)} \qquad (20)$$

For a uniform fractal, with all p_i equal (not a multifractal), one obtains a general dimension D_q that does not vary with q. For a non-uniform fractal, (multifractal) however, the variation of D_q with q quantifies the non uniformity. For instance

$$D_{\infty} = \lim_{l \to 0} \frac{\ln\left(\max_i p_i\right)}{\ln l} \tag{21}$$

$$D_{-\infty} = \lim_{l \to 0} \frac{\ln\left(\min_i p_i\right)}{\ln l}. \tag{22}$$

For a multifractal the D_qs are positive numbers which decrease monotonicly with q and for simple (one-scaled) fractals all the D_qs coincide.

Now, assume the following scaling relation for the probability of the i'th box in the limit $l \to 0$

$$p_i \propto l^{\alpha_i} \tag{23}$$

where α_i is position independent. This relation defines the *scaling index* α_i also called the *crowding index* or the *Lipschitz-Hölder exponent*. Since α controls the singularity of the density, it may also be called the *exponent of the singularity*. The same scaling relation can be found in many boxes (for small l), and all boxes with the same scaling index are said to be a sub-fractal with a pointwise dimension α_i. This sub-fractal is said to have a dimension $f(\alpha_i)$. In other words, the function $f(\alpha)$ can be interpreted as the Hausdorff dimension of the set of points with the same pointwise dimension α. For a simple fractal like the one scaled Cantor set the function $f(\alpha)$ is only defined in a single point $(\alpha, f) = (D_0, D_0)$ (see example below). Such a fractal is not a multifractal. In contrast, for multifractals α is no longer unique but may take on values in a finite range $[\alpha_{min}, \alpha_{max}]$, while $f(\alpha)$ turns out to be, in general, a single humped function with D_0 as its maximum. To find the relationship between $f(\alpha)$ and $\tau(q)$ we reexpress the partition sum as an integral in α. We then get

$$\Gamma(\tau, q) = \int d\alpha' \mu(\alpha') \cdot l^{q\alpha' - f(\alpha')} \tag{24}$$

where $d\alpha' \mu(\alpha') \cdot l^{q\alpha' - f(\alpha')}$ is the number of times α' assumes a value in the interval $[\alpha', \alpha' + d\alpha']$. In the limit $l \to 0$, the dominant contribution to the integral is received when the exponent $q\alpha' - f(\alpha')$ is close to its minimum value, so we perform a saddle-point approximation

$$\frac{d}{d\alpha'}\left[q\alpha' - f(\alpha')\right]_{\alpha'=\alpha(q)} = 0 \qquad (25)$$

This leads to the following Legendre transformation [13], which is used to determine the $f(\alpha)$ spectrum

$$\begin{cases} \dfrac{d\tau}{dq} = \alpha \\ \tau(q) = \alpha q - f \\ \dfrac{df}{d\alpha} = q \\ \dfrac{d^2 f}{d\alpha^2} < 0 \end{cases} \qquad (26\text{ a-d})$$

From these equations we note that the function $f(\alpha)$ is a convex function with a slope q in each dense point. As $q \to \infty$ the largest p_i (i.e., the most concentrated part of the multifractal) dominate the partition function. This corresponds to the point where the $f(\alpha)$ curve vanishes with infinite slope, which is at the leftmost part for the minimum α. As $q \to -\infty$ the smallest p_i dominate (i.e., the least concentrated part) and the corresponding α-value, the rightmost part of the $f(\alpha)$ curve vanishes with negative infinite slope. By increasing (decreasing) the exponent q, boxes with higher (lower) probabilities, i.e., fractal regions with denser (more ramified) occupation, are selected. We then see that the contribution of the partition function of different powers of the box probabilities is dominated by a different fractal subset. For $q = 1$ the generalized dimension is of special importance. From the relation $(q-1)D_q = q\alpha_q - f_q$ and its derivative taken at $q = 1$ we find $D_1 = \alpha_1 = f_1$ where

$$D_1 = \lim_{l \to 0} \frac{1}{\ln l} \cdot \sum_{i=1}^{N(l)} p_i \cdot \ln p_i = \lim_{l \to 0} \frac{1}{\ln l} \cdot \left(-S(l)\right) \qquad (27)$$

The quantity D_1 thus measures how the information scales with *ln l*. Therefore D_1 is called the *information dimension* [18, 19]. The function *S(l)* is called the *entropy* of the fractal. Moreover, this concept has been used to give a precise definition of a multifractal [19]. A distribution is said to be a multifractal measure if its Hausdorff dimension D_0 exceeds its information dimension D_1. In a similar way one can show that the dimension D_2 measure the correlation between the probabilities p_i and is therefore called the *correlation dimension* of the set.

3.1: The box-counting method

In box-counting we cover the fractal with boxes of different sizes and count the number of particles in each box. For simplicity, we use boxes of equal size, $(1/2)^m$, $m = 1, 2, \ldots, m_p$ where $(1/2)^{m_p}$ is the size of the smallest particle in the fractal. We never use boxes of size smaller than the smallest particles, since this gives no new information. The probability p_i to find a particle in a box i is then given by the number of particles in the box, n_i, divided by the total number of particles in the fractal N. With known probabilities and box-size, we can construct the partition function, $\Gamma(\tau,q)$ Eq. (15) and calculate the fractal dimensions D_q, Eq. (19). From Eqs. (17) and (26 a) we get the scaling exponent

$$\alpha(q) = \frac{d\tau(q)}{dq} = \lim_{l \to 0} \frac{1}{\ln l} \cdot \frac{\sum_{i=1}^{N(l)} (p_i)^q \cdot \ln p_i}{\sum_{i=1}^{N(l)} (p_i)^q} \tag{28}$$

which is used with Eq. (18) to find the $f(\alpha)$-spectrum:

$$f(\alpha(q)) = q\alpha(q) - (q-1)D_q. \tag{29}$$

In section 3.6 we continue the discussion about box-counting by studying the snowflake fractal used in paper I and paper II. This box-counting algorithm is called fixed-size box-counting. Another possibility is to use an algorithm called the fixed-mass box-counting, which consists in evaluation of the required box size to accumulate an amount of measure $\mu \in [\mu_{min}, \mu_{max}]$. It is specially appropriate to the evaluation of multifractal indices with $q \leq 0$.

A pattern Fig. 12(a) is discretized and stored in a matrix Fig. 12(b) of pixels with unit area ($l_{min}^2 = 1$, in pixel units). The measure, μ is also discretized by assigning a real number p_i to each nonempty box. The measure contained in each box, centred at random in a real domain with real size l, takes into account the fraction of pixels that are embedded in it. For the box-counting fixed-size algorithm the procedure consists in covering the pattern with grids, randomly located, of several lengths l in order to have several values $p_i(l)$. For the box-counting fixed-mass algorithm the procedure consists in evaluating several lengths $l_i(p)$, of boxes randomly located in the aggregate which contain a measure p. When using box-counting on the snowflake multifractal below we will use the fixed-size algorithm for all values of q, and without moving the grid. One problem with fixed-size box-counting is that, since the boxes will not necessarily be centred on particles on the fractal, some of the boxes will contain spuriously small measure (probability), thus creating problems for negative q-values. This is a difficult problem when box-counting is used to calculate the $f(\alpha)$ spectrum for a general fractal, such as an aggregate.

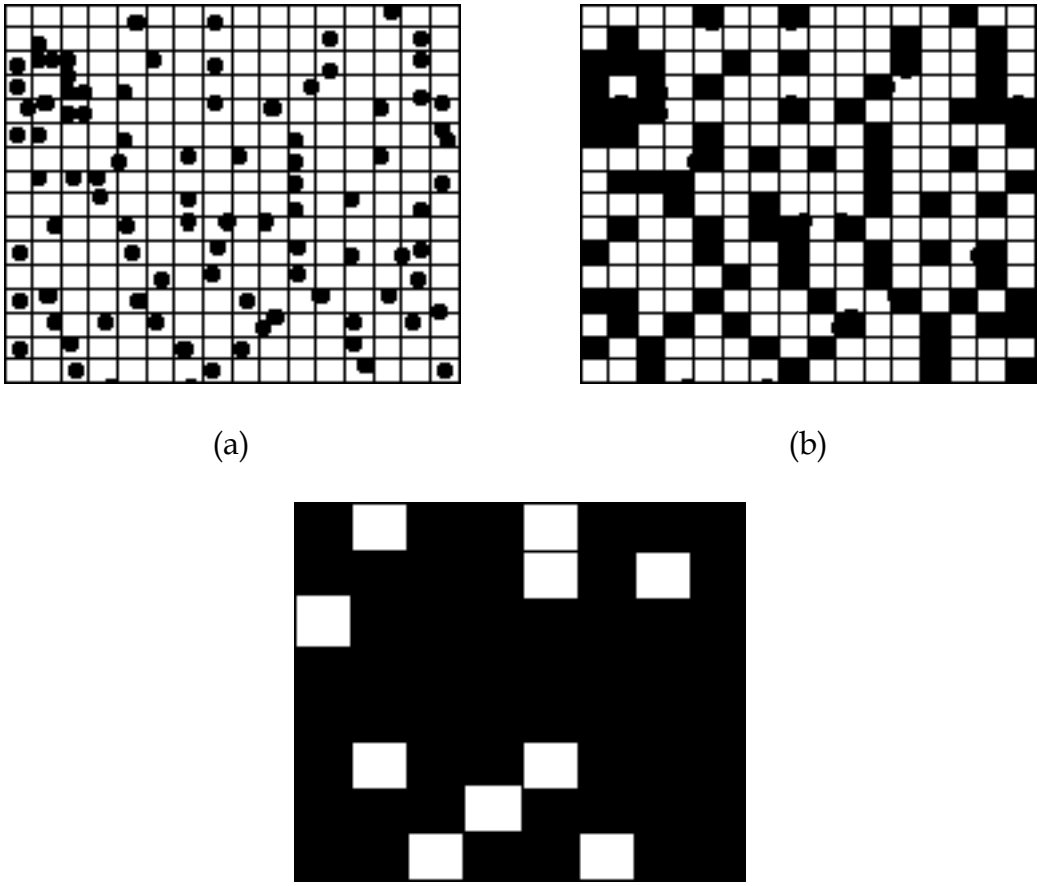

(a) (b)

(c)

Figure 12. In (a) we see a pattern with 89 particles in a grid of size 1/16. The mass of a particle is then normalized to be 1/89. Most of the boxes are empty but some contains one two or at most three particles. Figure (b) shows the boxes containing mass. The probability p_i in each box then vary between ≈ 1/89 to ≈ 3/89. At next box-level (c) the most of the boxes contains mass. For an accurate calculation the need of moving the original grid becomes of importance.

3.2: The one-scaled Cantor set (part 2)

To illustrate the difference between a simple fractal and a multifractal we begin by studying the one-scaled Cantor set. First we construct the partition-function Γ. Since the Cantor set at level n consist of 2^n intervals of size 3^{-n} the partition function is given by

$$\Gamma(q,\tau)=\sum_{i=1}^{2^n}\frac{(p_i^n)^q}{(l_i^n)^\tau}=\sum_{i=1}^{2^n}2^{-nq}\cdot 3^{n\tau}=1 \qquad (30)$$

To find the function $\tau(q)$ we take the logarithm of Eq. (30). We then get

$$-n\tau \cdot \ln 3 = \ln\left(\sum_{i=1}^{2^n} 2^{-nq}\right) = \ln\left(2^n \cdot 2^{-nq}\right) = (1-q)n \cdot \ln 2 \qquad (31)$$

i.e.,

$$\tau(q) = (q-1)\frac{\ln 2}{\ln 3} \qquad (32)$$

The generalized dimensions *Dq* is then given by Eq. (19), i.e.,

$$D_q = \frac{\ln 2}{\ln 3} \qquad (33)$$

which is the same as the Hausdorff dimension D_0 found in section 2.2. From Eqs (26a) and (32) we get the scaling exponent α

$$\alpha = \frac{\ln 2}{\ln 3} \qquad (34)$$

and finally from Eq. (26b) we get

$$f(\alpha) = \frac{\ln 2}{\ln 3} \qquad (35)$$

i.e., $\alpha = f(\alpha) = D_q = D_0$ as we expected for a one-scaled fractal.

3.3: The two-scaled Cantor set

To get a non-trivial $f(\alpha)$ spectrum we will next consider the simplest multifractal we can imagine, namely a two-scaled Cantor set as shown in Fig. 13. The set is constructed by dividing the unit interval in two pieces of different lengths, $L = 1/2$ and $l = 1/4$, respectively, and repeating the dividings self-similarly ad infinitum. The measures (probabilities) of the intervals are then $P = 2/3$ and $p = 1/3$ (if $p_i \sim l_i$).

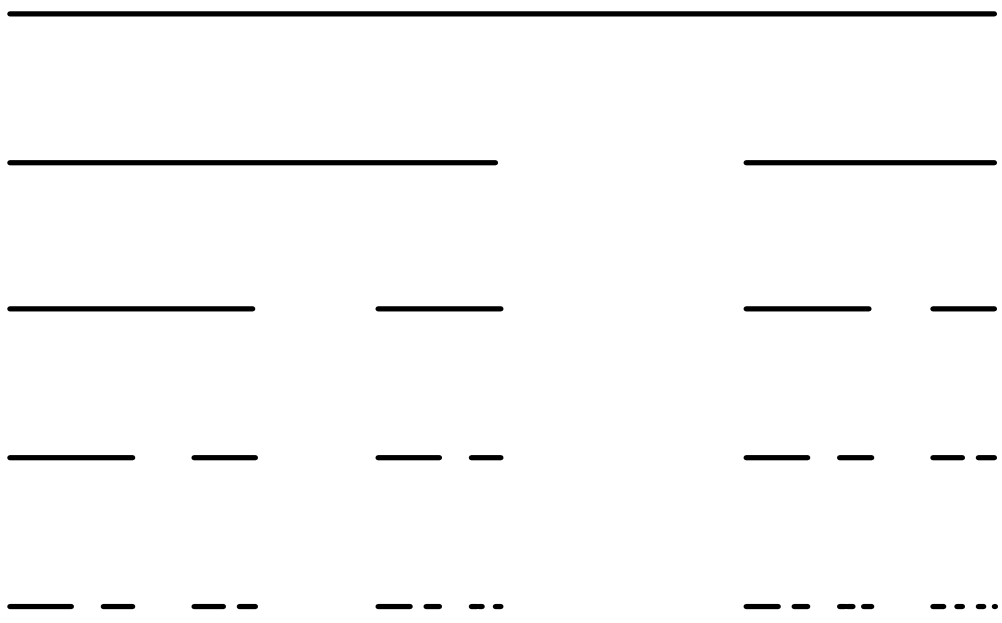

Figure 13. A Cantor set construction with two rescalings L = 1/2 and l = 1/4 with probabilities P = 2/3 and p = 1/3. The division of the set continues self-similarly ad infinitum.

The partition function Γ at the first level of construction, i.e., for *n = 1* is given by

$$\Gamma_1(L,l,P,p) = \frac{P^q}{L^\tau} + \frac{p^q}{l^\tau} \tag{36}$$

Similarly, at the next level Γ will be

$$\Gamma_2(L,l,P,p) = \left(\frac{P^q}{L^\tau}\right)^2 + 2\frac{P^q p^q}{L^\tau l^\tau} + \left(\frac{p^q}{l^\tau}\right)^2 = \left(\frac{P^q}{L^\tau} + \frac{p^q}{l^\tau}\right)^2 \tag{37}$$

and at a general level *n*, the partition function Γ, is given by

$$\Gamma_n(L,l,P,p) = \left(\frac{P^q}{L^\tau} + \frac{p^q}{l^\tau}\right)^n \tag{38}$$

The simple partition function is due to the recursive constructions of the Cantor set. Since we have a normalized measure ($P + p = 1$) the partition function $\Gamma_n = 1 \;\forall\; n$, i.e., Γ is independent of *n*. Such a partition function is called a *generator*. To find the $f(\alpha)$ spectrum for this set we first have to find the function $\tau(q)$ and then use the Legendre transformation Eqs. (26a) and (26b). The function $\tau(q)$ can be found by solving the equation

$$\frac{P^q}{L^\tau} + \frac{p^q}{l^\tau} = 1 \tag{39}$$

with Newton-iterations. If the probabilities (*P* and *p*) are proportional to the respective length (*L* and *l*) i.e., *P = L/(L + l)* and *p = l/(L + l)*, equation can be reexpressed as a second order polynomal and then we can find an analytical expression of $\tau(q)$ (see below). If we assume $P > p$ the first term of Eq. (39) dominates for large positive *q*-values. We then have

$$\tau(q \to \infty) = q \cdot \frac{\ln P}{\ln L} \tag{40}$$

and

$$f(\alpha) = \alpha q - \tau(q) = q \cdot \frac{d\tau(q)}{dq} - \tau(q) \equiv 0 \tag{41}$$

similarly, for large negative *q*:s, the second term of Eq. (39) dominates, i.e.,

$$\tau(q \to -\infty) = -|q| \cdot \frac{\ln p}{\ln l} \tag{42}$$

and $f(\alpha) = 0$. The generalized dimensions in these limits are given by

$$D_\infty = \frac{\ln P}{\ln L} \tag{43}$$

and

$$D_{-\infty} = \frac{\ln p}{\ln l} \tag{44}$$

From the analysis above and the fact $\tau(1) = 0$ (see Eq. (17)), we can now plot the shape of $\tau(q)$, D_q and $f(\alpha)$ (see paper I). In general those curves look like the curves in Fig. (14) - (16).

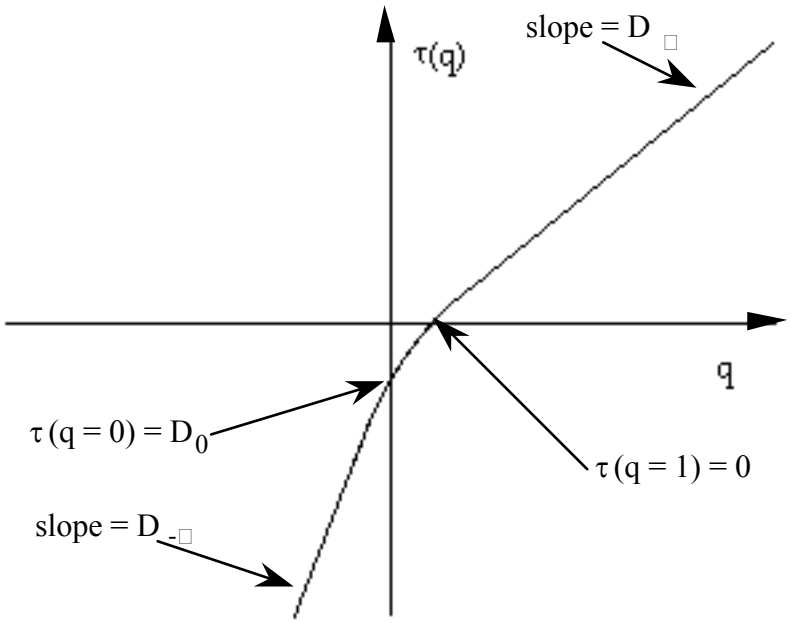

Figure 14 The general shape of the function τ(q). For large negative q-values τ(q) = q . D-∞ - f-∞ and for large positive q:s τ(q) = q . D∞ - f∞. Remark D-∞ = αmin and D∞ = αmax.

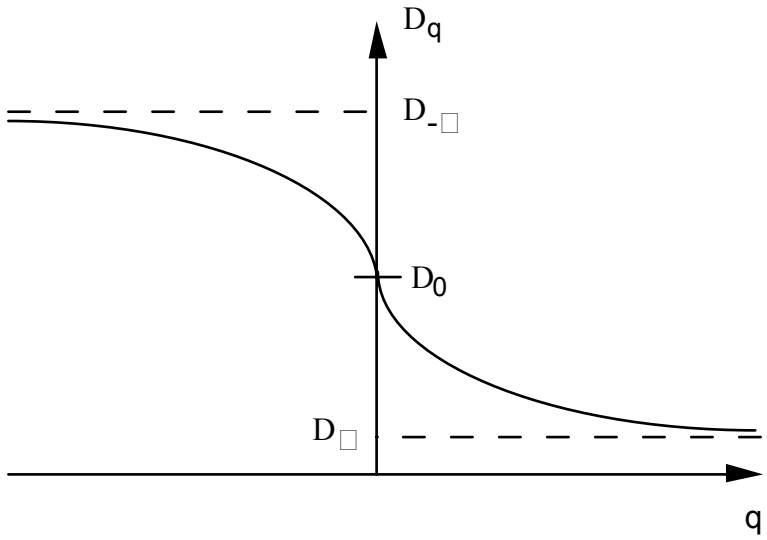

Figure 15. The general shape of the function Dq, D0 = fmax.

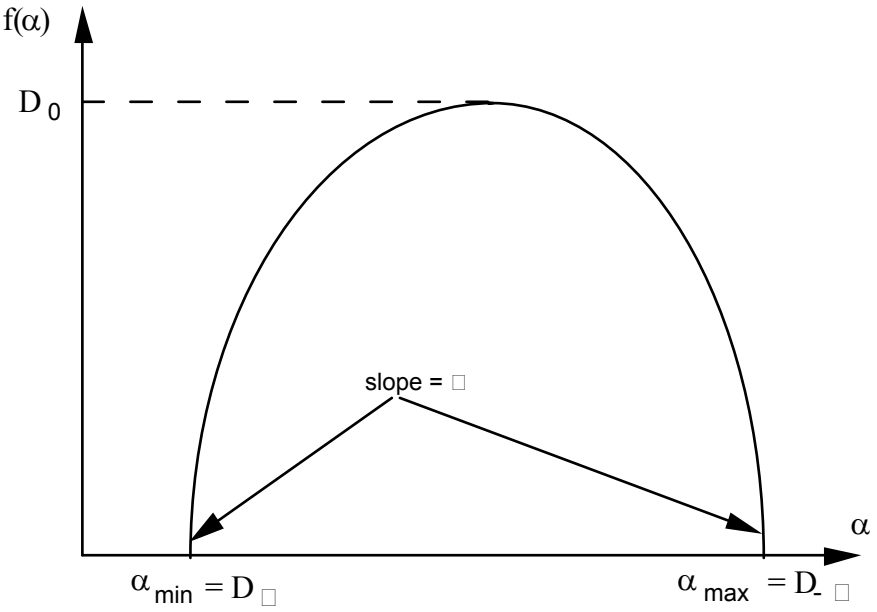

Figure 16. The general shape of the function f(α).

In the first step of the Cantor set construction, the set consists of tree parts, a large interval *L*, a hole *h* and a small interval *l*. We denote this set by (*L, h, l*) or just (*L, l*). The next generation can be constructed by a multiplication:

$$(L + l)\cdot(L + l) = L^2 + Ll + lL + l^2. \qquad (45)$$

This set is denoted by (L^2, $2Ll$, l^2). The length of each interval is given since $L = 1/2$ and $l = 1/4$. The next generation is given by (L^3, $3L^2l$, $3Ll^2$, l^3) and so on. We now observe that the Cantor set at level *n* only consists of $n + 1$ different scales. We also observe that the number of boxes of size 2^{-n} (= the size of the largest interval) is a Fibonacci number and we can calculate the Hausdorff dimension by studying two nearby levels $m - 1$ and *m*. The Fibonacci numbers are defined by

$$F_n = F_{n-1} + F_{n-2} \qquad \text{with} \quad F_0 = 0, F_1 = 1. \qquad (46)$$

The Fibonacci numbers are closely related to the golden mean

$$\nu = \frac{1}{2}(1 + \sqrt{5}). \qquad (47)$$

We have in particular

$$F_n \xrightarrow[n\to\infty]{} \left(\frac{1+\sqrt{5}}{2}\right)^n \qquad (48)$$

Since the partition functions Γ_m and Γ_{m-1} have to be equal we can then use $F_m / F_{m-1} \to \left(\sqrt{5}+1\right)/2$ as $m \to \infty$ to find D_0. This gives

$$F_m \cdot 2^{-m\cdot\tau(0)} = F_{m-1} \cdot 2^{-(m-1)\tau(0)} \tag{49}$$

and

$$D_0 = -\tau(0) = \frac{1}{\ln 2} \cdot \ln\left\{\frac{\sqrt{5}+1}{2}\right\} \tag{50}$$

which is the same result as was found in paper I.

3.4: Exactly solvable recursive sets

There exists a set of recursive multifractal objects which are exactly solvable. We will in this section study such sets with two rescalings. The partition function for a general two-scaled recursive set is given by

$$\Gamma(L,l,P,p) = N \cdot \frac{P^q}{L^\tau} + n \cdot \frac{p^q}{l^\tau} \tag{51}$$

where N is the number of segments of length L with probability P and n the number of segments of length l with probability p on the first level of construction. This equation is exactly solvable if $l = L^2$ (< 1) and if the probabilities P and p are proportional to their respective length and normalized i.e., $NP + np = 1$. Then $\Gamma = 1$ and

$$P = \frac{L^d}{N \cdot L^d + n \cdot L^{2d}} \tag{52}$$

and

$$p = \frac{L^{2d}}{N \cdot L^d + n \cdot L^{2d}} \tag{53}$$

where d is the topological dimension of the set. From the expression (51) for the partition function one gets

$$N \cdot L^{dq-\tau} + n \cdot L^{2\cdot(dq-\tau)} - \left(N \cdot L^d + n \cdot L^{2d}\right)^q = 0 \tag{54}$$

This equation can be reexpressed as a second order polynomal If we set $x = L^{dq - \tau}$, we get

$$x^2 + \frac{N}{n} \cdot x - \frac{\left(N \cdot L^d + n \cdot L^{2d}\right)^q}{n} = 0. \qquad (55)$$

Equation (55) has a positive and a negative root. We ignore the negative one since a negative length is irrelevant. The positive root is

$$x = L^{dq-\tau} = \frac{\sqrt{N^2 + 4n \cdot (N \cdot L^d + n \cdot L^{2d})^q} - N}{2n} \qquad (56)$$

Finally, we take the logarithm of Eq. (56). We then get the expression for the function $\tau(q)$.

$$\tau(q) = dq - \frac{1}{\ln L} \cdot \ln\left\{\frac{\sqrt{N^2 + 4n \cdot (N \cdot L^d + n \cdot L^{2d})^q} - N}{2n}\right\} \qquad (57)$$

The generalized dimensions D_q are given by Eq. (18). Specially for the Hausdorff dimension we get

$$D_0 = \frac{1}{\ln L} \cdot \ln\left\{\frac{\sqrt{N^2 + 4n} - N}{2n}\right\} \qquad (58)$$

We also get the limits of D_q as

$$D_{-\infty} = d - \frac{\ln\left(N \cdot L^d + n \cdot L^{2d}\right)}{2 \cdot \ln L} \qquad (59)$$

and

$$D_{\infty} = d - \frac{\ln\left(N \cdot L^d + n \cdot L^{2d}\right)}{\ln L} \qquad (60)$$

From the Legendre transformation (Eq. (26)) we also have the $f(\alpha)$-spectrum

$$\alpha(q) = d - \frac{2n \cdot \left(N \cdot L^d + n \cdot L^{2d}\right)^q \cdot \ln\left(N \cdot L^d + n \cdot L^{2d}\right)}{\ln L} \cdot \left[N^2 + \right.$$
$$\left. + 4n \cdot \left(N \cdot L^d + n \cdot L^{2d}\right) - N \cdot \sqrt{N^2 + 4n \cdot \left(N \cdot L^d + n \cdot L^{2d}\right)^q}\right]^{-1} \qquad (61)$$

and

$$f(\alpha(q)) = q \cdot \alpha(q) - \tau(q) \qquad (62)$$

If we apply Eqs. (47) - (62) on the two-scaled Cantor set where *l = 1/2, N = n = 1* and *d = 1* we find

$$\tau(q) = q + \frac{1}{\ln 2} \cdot \ln\left\{ \frac{\sqrt{1 + 4 \cdot (3/4)^q} - 1}{2} \right\} \tag{63}$$

The Hausdorff dimension is then given by

$$D_0 = \frac{1}{\ln 2} \cdot \ln\left\{ \frac{\sqrt{5} - 1}{2} \right\} \tag{64}$$

and the limits of the generalized dimension by

$$D_{-\infty} = 1 + \frac{\ln(3/4)}{2 \cdot \ln 2} = \frac{\ln(3)}{\ln 4} \tag{65}$$

and

$$D_{\infty} = 1 + \frac{\ln(3/4)}{\ln 2} = \frac{\ln(3/2)}{\ln 2} \tag{66}$$

Finally, the $f(\alpha)$ spectrum is given by

$$\alpha(q) = 1 - \frac{4 \cdot (3/4)^q}{1 + 4 \cdot (3/4)^q - \sqrt{1 + 4 \cdot (3/4)^q}} \tag{67}$$

and

$$f(\alpha(q)) = \frac{4q \cdot (3/4)^q}{1 + 4 \cdot (3/4)^q - \sqrt{1 + 4 \cdot (3/4)^q}} - \frac{1}{\ln 2} \cdot \ln\left\{ \frac{1 + 4 \cdot (3/4)^q - \sqrt{1 + 4 \cdot (3/4)^q}}{2} \right\} \tag{68}$$

The generalized dimensions *Dq* and the $f(\alpha)$ spectrum for this Cantor set is shown in paper I.

A general recursive fractal set with a finite number, N of rescalings

$$\Gamma = \sum_{i=1}^{N} n_i \frac{p_i^q}{l_i^{\tau}} = 1 \tag{69}$$

can be solved by Newton iterations. For each value of q we then solve Eq. (69) to find the function $\tau(q)$.

3.5: The snowflake fractal

Another solvable multifractal is shown in Fig. 17 a-b We call this multifractal a two-scaled snowflake fractal since it reminds of a snowflake. This fractal is investigated in paper (II) and can be used in the study of fractal aggregates.

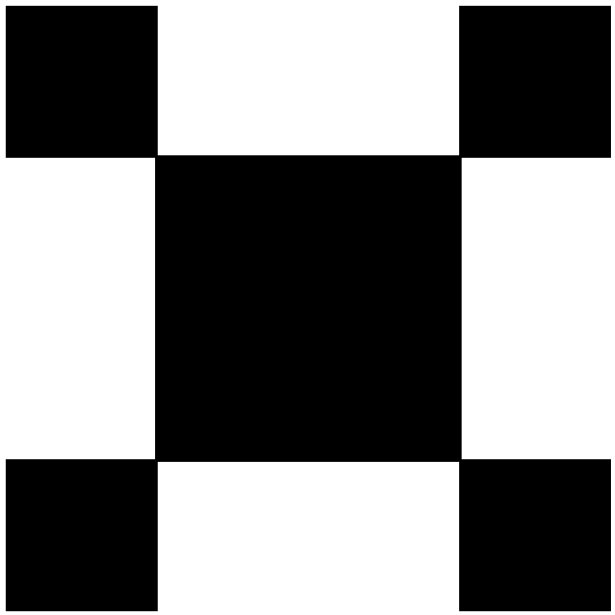

Figure 17 a. The first level of construction of a two-scaled snowflake fractal

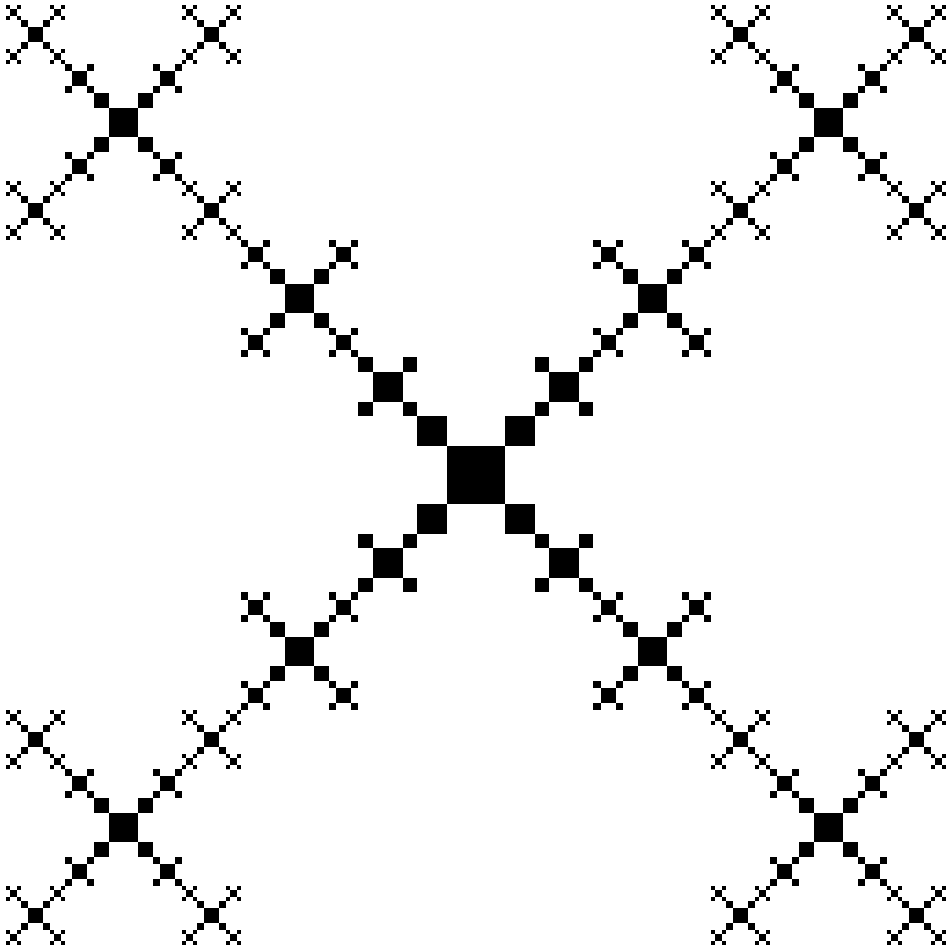

Figure 17 b The fourth level of construction of a two-scaled snowflake fractal

3.6: Box-counting on the snowflake fractal

In this section the snowflake multifractal will be analysed in more detail. From this example we learn a lot about box-counting. In paper II we show that it is possible to find analytic expressions for the box-counting solution on any level of construction n, and for any level of grids m, i.e., box-sizes $l = 2^{-m}$. Fig. 17a shows the multifractal at the first level of construction. If we call the "*particle size*" the size of the smallest square in the set, the number of particles will increase as 8^n. The fractals in Fig. 17a then consists of 8 particles of size $1/4$ (a) and $8^2 = 64$ particles of size $(1/4)^2 = 1/16$ (b) respectively.

The snowflake fractal is covered with boxes of size $(1/2)^m$, $m = 1, 2, ..., m_n$ where $(1/2)^{m_n} \equiv (1/4)^n = l^n$ is the size of the smallest square in the fractal. The largest square (the one in the centre) has the size $L^n = (1/2)^n$. We then calculate the probability p_i i.e., the measure of the fractal in each box i.

First we have to find a recursive rule to construct the snowflake fractal at any level. In paper II we defined the operator $\hat{T}$ operating on a square x by

$$\hat{T}x = 4xl + xL. \qquad (70)$$

If we let this operator act on a unit square, i.e., $x \equiv 1$ we get $4l + L$, where l is a new square of size $1/4$ and L a new square if size $1/2$. By repeated operation with $\hat{T}$ on the new set $(4l + L)$ we construct any level of the fractal. On the fourth level (Fig. 17b) we have

256	squares of size *1/256*:	$256\ l^4$
256	squares of size *1/128*:	$64\ l^3L$, $64\ lLl^2$, $64\ Ll^3$ and $64\ L^2lL$
96	squares of size *1/64*:	$16\ l^2L^2$, $16\ lLlL$, $16\ Ll^2L$, $16\ lL^2l$, $16\ LlLl$ and $16\ L^2l^2$
16	squares of size *1/32*:	$4\ lL^3$, $4\ LlL^2$, $4\ L^2lL$ and $4\ L^3l$, and
1	square of size *1/16*:	L^4.

To calculate the fractal dimensions D_q and the $f(\alpha)$ spectrum we need to find the function $\tau(q)$

$$\tau(q)^{(m)} = -\frac{1}{m \ln 2} \ln\left\{ \sum_{i=1}^{N} a_i^{(m)} \left\{ p_i^{(m)} \right\}^q \right\} \qquad (71)$$

for all n and m, where the coefficients $a_i^{(m)}$ are the number of boxes with the same probability $p_i^{(m)}$.

To find the coefficients we have to study the snowflake for some levels and the possible box coverings. In Fig. 18 we show the snowflake on level $n = 2$ and box levels $m = 4, 3, 2$ and 1. On this level the smallest particle have the length $(1/4)^2 = 1/16$. In the finest box resolution $m = 4$ we have 64 boxes all with the same probability $p = 1/64$. The function(q) is then given by

$$\tau(q)_2^4 = -\frac{\ln\left\{64 \cdot (64)^{-q}\right\}}{4 \ln 2} = -\frac{6 \ln 2 - 6q \ln 2}{4 \ln 2} = \frac{3}{2}(q-1)$$

which gives

$$\left(D_q\right)_2^4 = \frac{\tau(q)_2^4}{q-1} = \frac{3}{2},$$

$$\alpha(q)_2^4 = \frac{d}{dq}\,\tau(q)_2^4 = \frac{3}{2}$$

and

$$f(q)_2^4 = q \cdot \alpha(q)_2^4 - \tau(q)_2^4 = \frac{3}{2}$$

The values of the dimensions above are the first approximation of the exact values which are given in the limit $n \to \infty$ and $m \to \infty$. Due to the small box-size we only get one value of the probability and then only one value of the fractal dimensions, D_q, α and $f(\alpha)$ independent of the momentum q. If we increase the box size a factor *1/2* we find the same result for the dimensions since we then get *256* filled boxes of size *1/32* with probability *1/256*. This shows that the smallest box-size of interest is the same as the smallest particle.

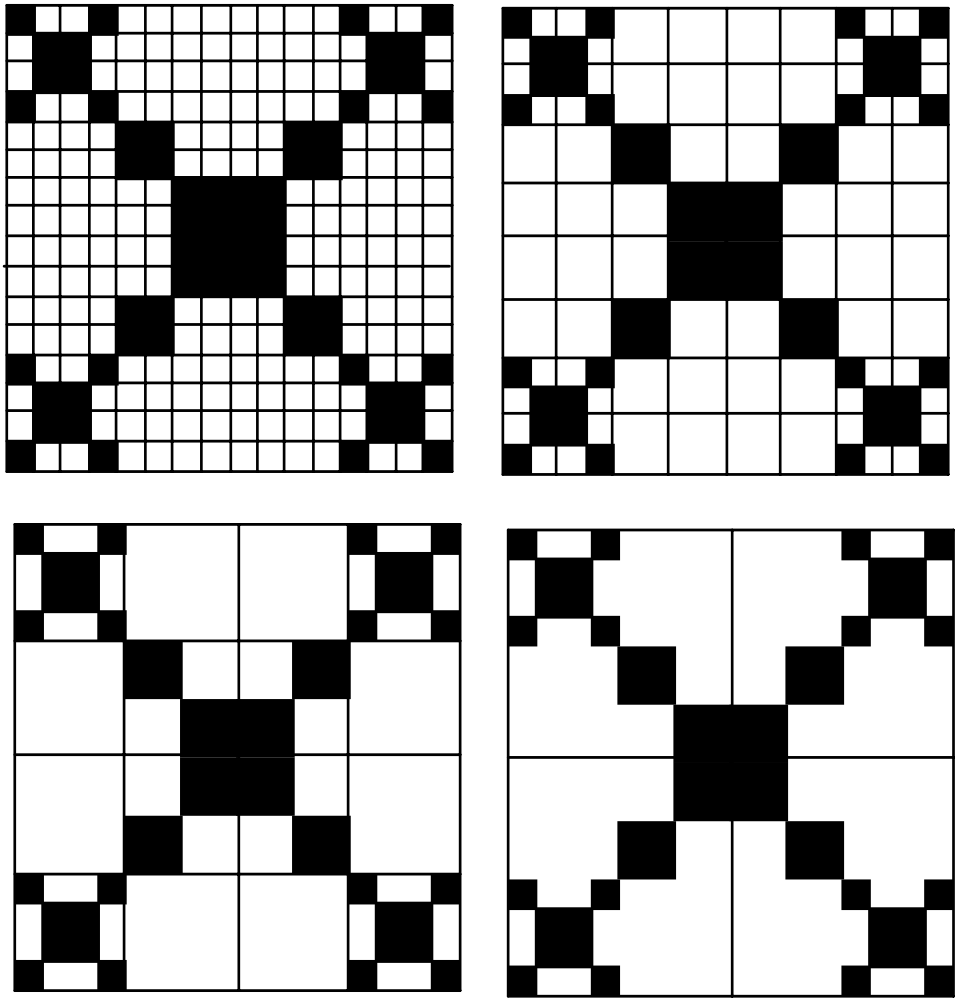

Figure 18. This is the fractal at level n = 2 covered by boxes of level m = 4, 3, 2 and 1, i.e., the particle sizes is l = (1/4)^2 = 1/16 and the box sizes are (1/2)^4 = 1/16, (1/2)^3 = 1/8, (1/2)^2 = 1/4 and (1/2)^1 = 1/2 respectively.

If we decrease the box size to level, *m = 3* we have *16* boxes with probability *2/64* and 8 boxes with probability *4/64 = 1/16*. The function *τ(q)* then becomes

$$\tau(q)_2^3 = -\frac{1}{3\ln 2}\ln\left\{16\cdot 32^{-q} + 8\cdot 16^{-q}\right\}$$

which gives a continuous function of generalized dimensions with

$$\left(D_0\right)_2^3 = -\tau(0)_2^3 = \frac{\ln 24}{3\ln 2} = 1.5283\ldots$$

and the limits

$$\left(D_{-\infty}\right)_2^3 = 1.6667\ldots$$

$$\left(D_{\infty}\right)_2^3 = 1.3333\ldots$$

when $q \to \pm\infty$. The *f(α)*-spectrum in the same limits are given by

$$\alpha(q)_2^3\Big|_{q\to-\infty} = \frac{d}{dq}\,\tau(q)_2^3\Big|_{q\to-\infty} = \frac{5}{3} = 1.6667\ldots$$

$$\alpha(q)_2^3\Big|_{q\to\infty} = \frac{d}{dq}\,\tau(q)_2^3\Big|_{q\to\infty} = \frac{4}{3} = 1.3333\ldots$$

and

$$f(q)_2^3 = q\cdot\alpha(q)_2^3 - \tau(q)_2^3$$

The next two levels (*m = 2* and *m = 1*) gives the same results as level *2* and *1* for the snowflake at level *n = 3* below.

Let us study one more level of the snowflake fractal, level *n = 3*. In Fig. 19 we show the upper left part of the snowflake with box level *m = 6*. On this level the snowflake consists of *512* particles of size *1/64*. The function *τ(q)* is then given by

$$\tau(q)_3^6 = \frac{3}{2}(q-1).$$

This gives the generalized dimensions

$$\left(D_q\right)_3^6 = \frac{\tau(q)_3^6}{q-1} = \frac{3}{2},$$

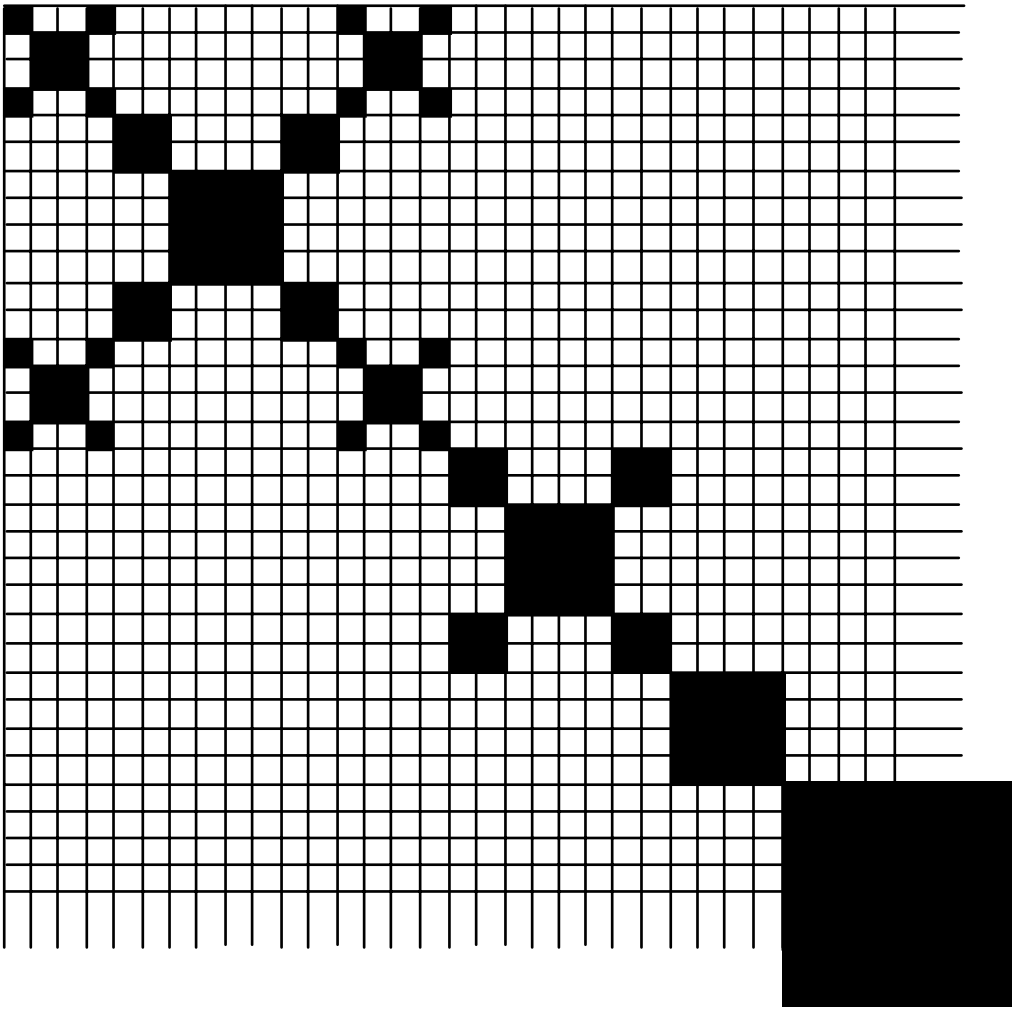

Figure 19. This is the upper left part of the snowflake fractal at level n = 3, covered by boxes of level m = 6, i.e., the smallest particles have the length l = (1/4)³ = 1/64 which is equal to the box size (1/2)⁶ = 1/64. The largest particle, in the middle have the size L = (1/2)³.

and the $f(\alpha)$-spectrum

$$\alpha(q)_3^6 = \frac{d}{dq}\,\tau(q)_3^6 = \frac{3}{2}$$

and

$$f(q)_3^6 = q \cdot \alpha(q)_3^6 - \tau(q)_3^6 = \frac{3}{2}.$$

When increasing the box size to level *m = 5, 4, 3* and *2*, Fig. 19 i.e., boxes of size *l = 1/32, 1/16, 1/8, 1/4* and *1/2* we get the following results

$$\tau(q)_3^5 = -\frac{1}{5\ln 2}\ln\left\{64\cdot 256^{-q} + 96\cdot 128^{-q}\right\}$$
$$\tau(q)_3^4 = -\frac{1}{4\ln 2}\ln\left\{48\cdot 64^{-q} + 8\cdot 32^{-q}\right\}$$
$$\tau(q)_3^3 = -\frac{1}{3\ln 2}\ln\left\{16\cdot 32^{-q} + 8\cdot 16^{-q}\right\}$$
$$\tau(q)_3^2 = \frac{3}{2}(q-1)$$

which gives continuous functions of general dimension D_q (except for box-level *m = 2* where all dimensions are the same). The Hausdorff dimension on each levels are given by

$$(D_0)_3^5 = -\tau(0)_3^5 = \frac{\ln 160}{5\ln 2} = 1.4644\ldots$$
$$(D_0)_3^4 = -\tau(0)_3^4 = \frac{\ln 56}{4\ln 2} = 1.4518\ldots$$
$$(D_0)_3^3 = -\tau(0)_3^3 = \frac{\ln 24}{3\ln 2} = 1.5283\ldots$$
$$(D_q)_3^2 = \frac{\tau(q)_3^2}{q-1} = \frac{3}{2}$$

and the limits by

$$(D_{-\infty})_3^5 = 1.6$$
$$(D_{\infty})_3^5 = 1.4$$

$$(D_{-\infty})_3^4 = 1.5$$
$$(D_{\infty})_3^4 = 1.25$$

$$(D_{-\infty})_3^3 = 1.6667\ldots$$
$$(D_{\infty})_3^3 = 1.3333\ldots$$

as $q \to \infty$ and $q \to -\infty$ respectively. The *f(α)*-spectrum is also a continuous functions, with limits

$$\alpha(q)_3^5\Big|_{q\to-\infty} = \frac{d}{dq}\,\tau(q)_3^5\Big|_{q\to-\infty} = \frac{8}{5} = 1.6$$

$$\alpha(q)_3^5\Big|_{q\to\infty} = \frac{d}{dq}\,\tau(q)_3^5\Big|_{q\to\infty} = \frac{7}{5} = 1.4$$

$$\alpha(q)_3^4\Big|_{q\to-\infty} = 1.5$$
$$\alpha(q)_3^4\Big|_{q\to\infty} = 1.25$$

$$\alpha(q)_3^3\Big|_{q\to-\infty} = 1.6667\ldots$$
$$\alpha(q)_3^3\Big|_{q\to\infty} = 1.3333\ldots$$

$$\alpha(q)_3^2 = \frac{d}{dq}\,\tau(q)_3^2 = \frac{3}{2}$$

The functions *f(q)* are given by

$$f(q)_3^m = q\cdot\alpha(q)_3^m - \tau(q)_3^m, \qquad m = 2, 3, 4, 5, 6.$$

On level $m = 1$ i.e., $l = 1/2$ we have *4* boxes with probability $128/512 = 1/4$. The function*(q)* is then given by

$$\tau(q)_3^1 = 2(q-1)$$

which gives

$$\left(D_q\right)_3^1 = \alpha(q)_3^1 = f(q)_3^1 = 2$$

In this limit all dimensions are equal to 2 since all boxes are filled and with the same probability.

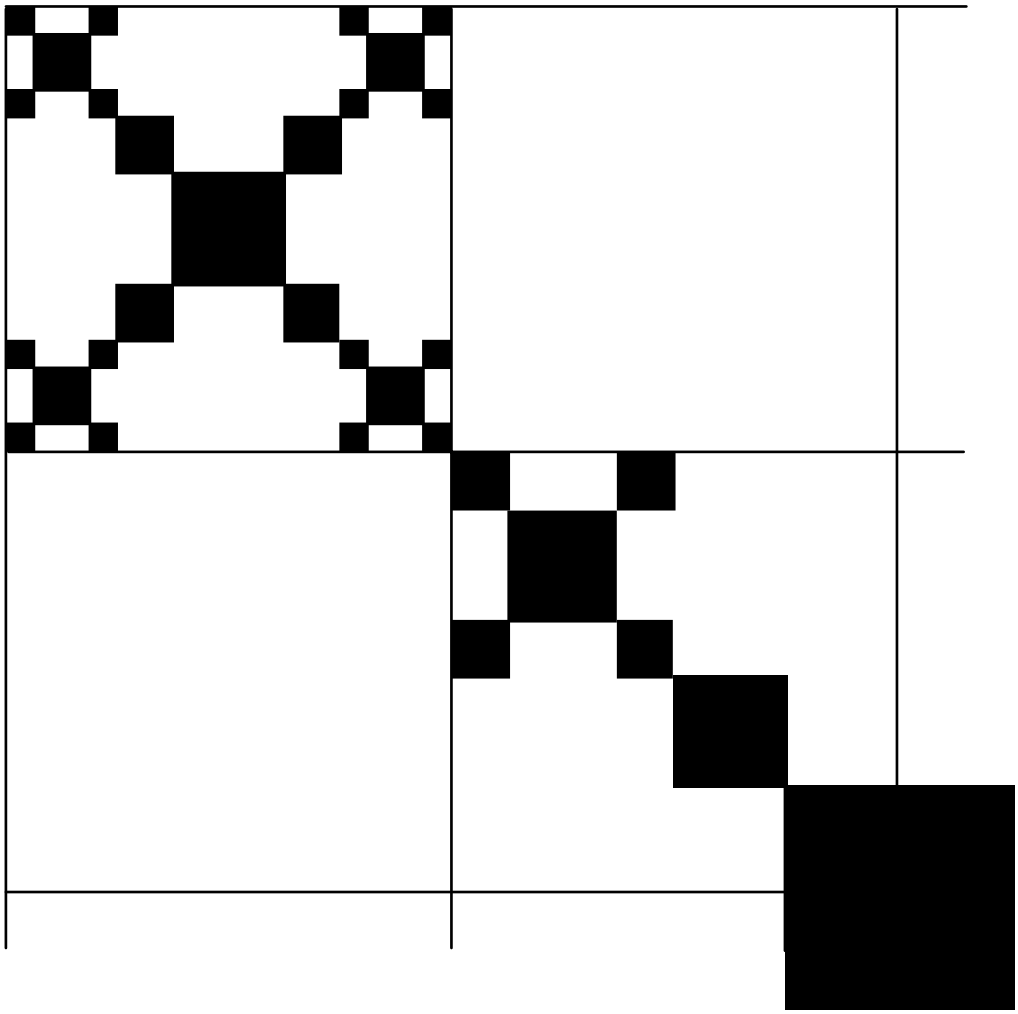

Figure 20. This is the upper left part of the fractal at level n = 3 covered by boxes of level m = 2, i.e., with boxes of size l = (1/2)^2 = 1/4.

To illustrate the behaviour of increasing box-size we construct *Table 1 - 3*. *Table 1* shows the behaviour when increasing the box-size in the fractal on level *n = 2* Fig. 18 where the first column represent the *64* filled boxes, *16* with one l^2-particle, *16* boxes with a quarter of a *lL*-particle, *16* boxes with a quarter of a *Ll*-particle and *16* where a L^2-particle cover *16* boxes. The next column represent the next box-size where each part of the *lL* particles lies in the same boxes as the l^2-particles and all parts of the four *Ll* particles moves into the same box and the L^2 particle now cover four boxes. We then have 16 boxes containing $l^2 + (1/4)lL$ four boxes containing *Ll* and four boxes of $(1/4)L^2$. At the next level we have *4* boxes of $4l^2 + lL$ and four with $Ll + (1/4)L^2$. In the last level we have four boxes containing $4l^2 + lL + Ll + (1/4)L^2$.

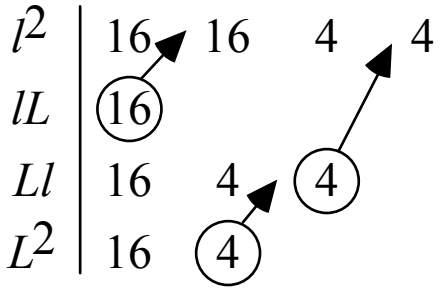

Table 1. This is the behaviour when decreasing the box size on the level n = 2 snowflake fractal, Fig. 18. The columns shows the contents in the "filled" boxes of sizes (1/16), (1/8), (1/4) and (1/2) respectively.

Table 2 and *3* show the same decrease of the box size for the snowflake fractal at level $n = 3$ and $n = 4$ respectively.

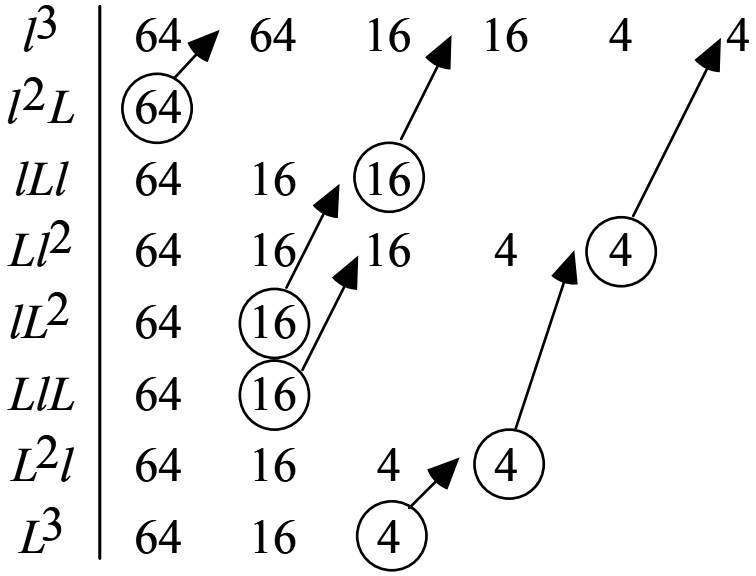

Table 2. This is the behaviour when decreasing the box size on the level n = 3 fractal,. The columns shows the contents in the "filled" boxes of sizes (1/64), (1/32), (1/16), (1/8), (1/4) and (1/2) respectively.

We can see from *Table 1 - 3* that the number of boxes containing the same set of particles can be written as $c \cdot 4^b$ see *Table 4*. A study of the contents in the boxes shows that the coefficient $a_i^{(m)}$ are given by

$$a_i^{(j)} = c_i^{(j)} \cdot 4^{b_i^{(j)}} \tag{72}$$

where we can find recursive rules for $c_i^{(j)}$ and $b_i^{(j)}$, see the result in the appendix of Paper II.

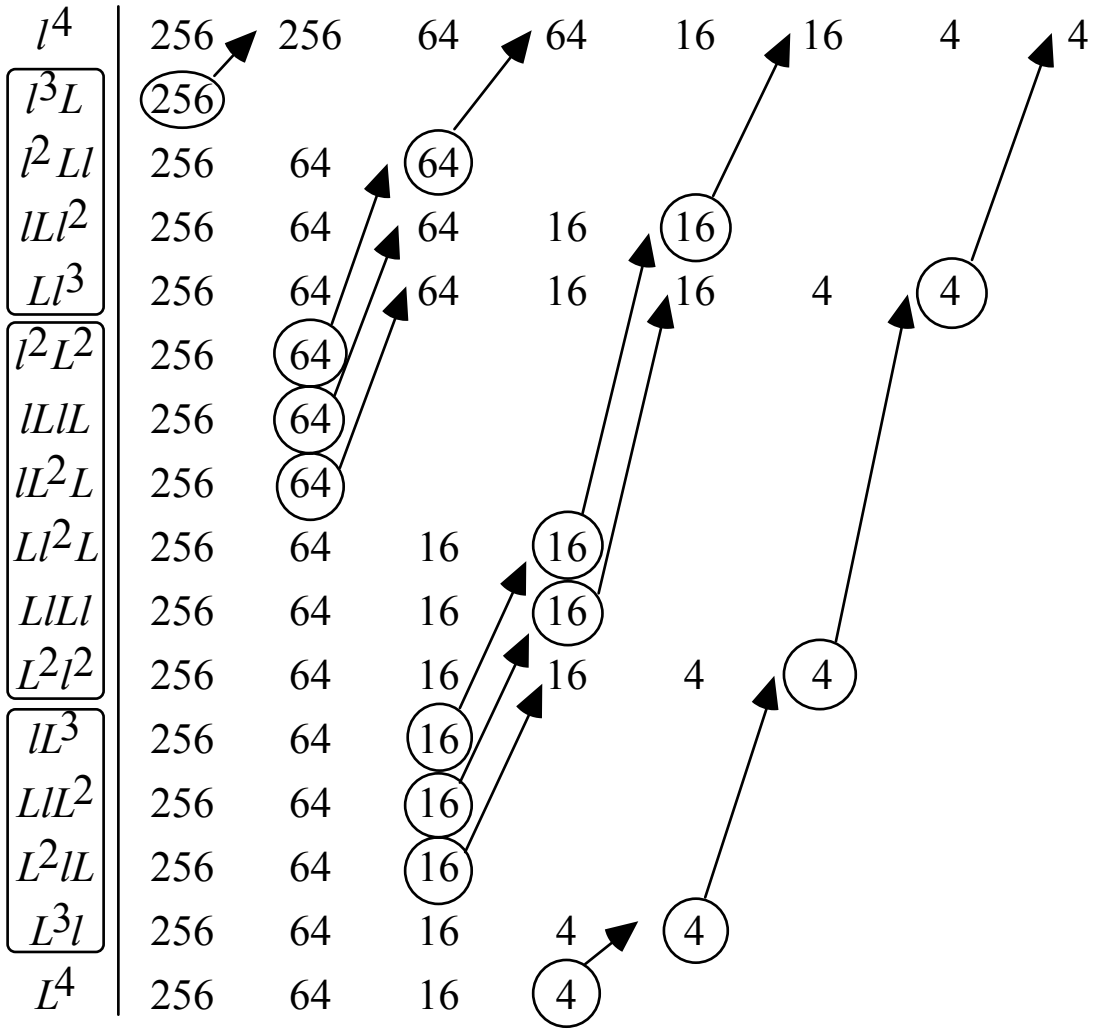

Table 3. This is the behaviour when decreasing the box size on the level n = 4 fractal. The columns show the contents in the "filled" boxes of sizes (1/256), (1/128), (1/64), (1/32), (1/16), (1/8), (1/4) and (1/2) respectively.

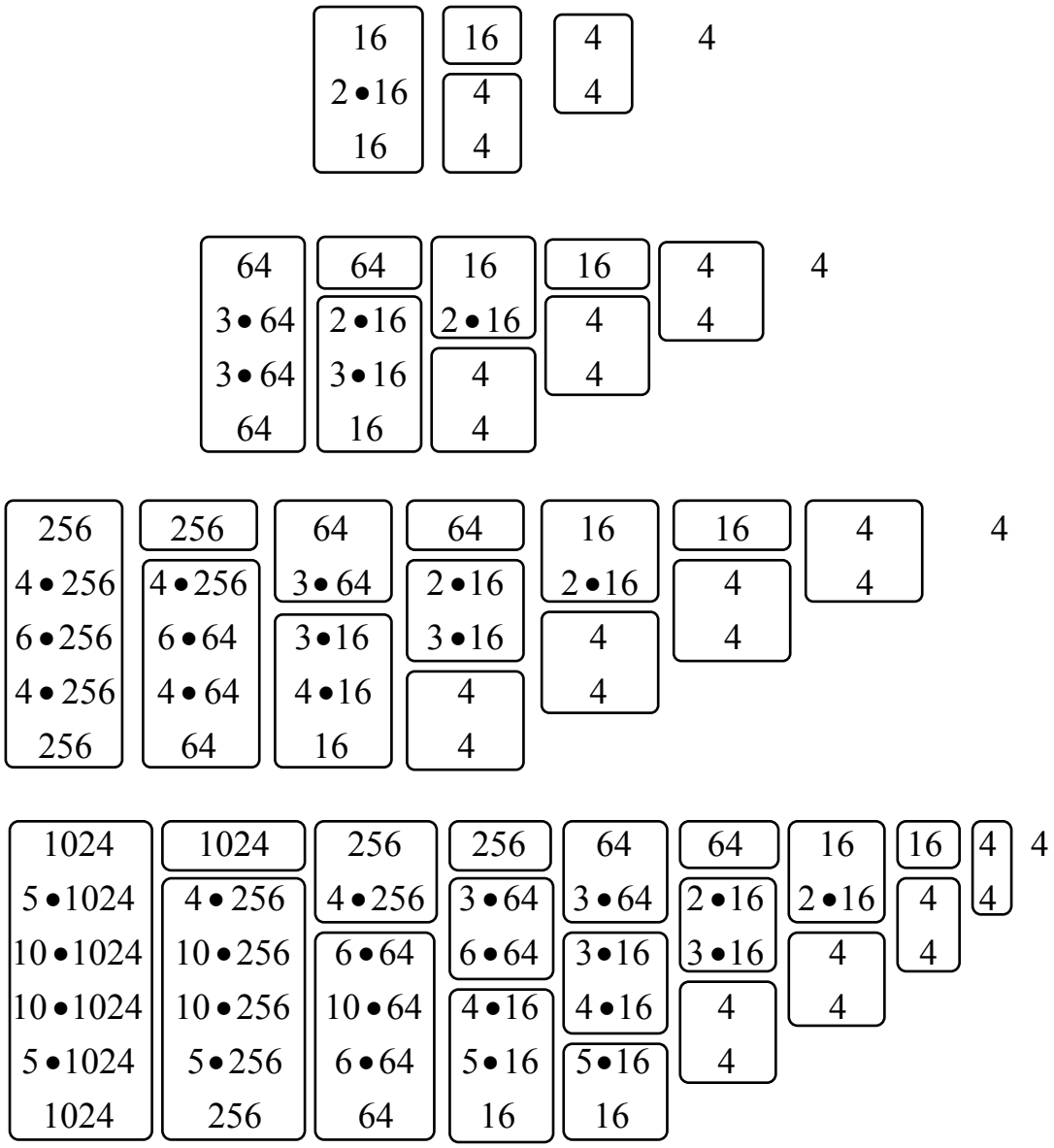

Table 4. This shows the coefficients for the fractal at level n = 2, 3, 4 and 5 with the possible box levels m. The coefficients inside the boxes are coefficients with the same probability (measure).

If we bring the probabilities and the coefficients into the same table, Table 5 we see that we can find a similar recursive expression for the probabilities. The complete solution to the box-counting problem is presented in the appendix of paper II.

level n = 2

Coefficients:

4
4 4
16 4 4
16 32 16

Probabilities:

4
8 8
32 16 16
64 64 64

---

level n = 3

Coefficients:

4
4 4
16 4 4
16 32 4 4
64 32 48 16
64 192 192 64

Probabilities:

4
8 8
32 16 16
64 64 32 32
256 128 128 128
512 512 512 512

---

level n = 4

Coefficients:

4
4 4
16 4 4
16 32 4 4
64 32 48 4 4
64 192 48 64 16
256 192 384 256 64
256 1024 1536 1024 256

Probabilities:

4
8 8
32 16 16
64 64 32 32
256 128 128 64 64
512 512 256 256 256
2048 1024 1024 1024 1024
4096 4096 4096 4096 4096

Table 5. This shows the coefficients and the probabilities for the fractal at level n = 2, 3, and 4. This table is used to find recursive relation for the probabilities of the snowflake fractal.

The box-counting solution to the snowflake multifractal consist of two families. This is due to the box-sizes compared with the contents in the boxes. We call the different families, the odd and the even. The first box-size is odd and has the same size as the smallest particles. Next box-size is even, next odd, and so on. Each corner of the odd box-sizes consist of a boxes containing reduced copies of the whole fractal. This gives, for large negative q-values an exact value of α and therefore $D_{-\infty}$. In Fig. 21 - Fig. 28 the black curves are solution with box-sizes larger than the largest particle, that in the middle. The red curves are solutions with box-sizes smaller than the largest particle. The convergence of the solutions is discussed in detail in paper II. All solutions below are calculated from the fractal at level $n = 90$, i.e., the number of particles in the fractal is $4^{90} \approx 1.53 \cdot 10^{54}$. The curves in the even family are for box-levels $m = 10, 20, ..., 160$ and the odd families for levels $m = 9, 19, ..., 159$.

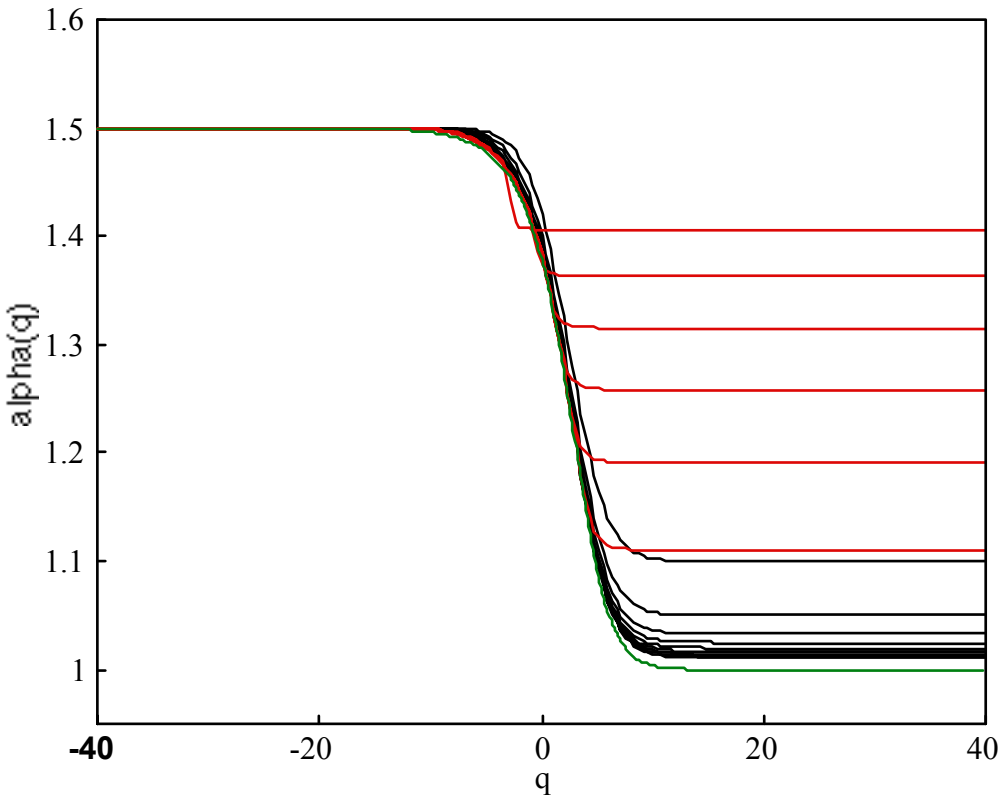

Figure 21. This is the function $\alpha(q)$ for the odd family. The black curves are solutions for boxes larger than the largest particle, the red curves are solutions for boxes smaller than the largest particle and the green is the exact solution.

This sets of solutions are compared with the exact solutions, the green curves, calculated from the analytical expressions Eq. (73) - (75) from paper I and II.

$$D_q(q) = \frac{1}{q-1} \cdot \left(2q + \frac{1}{\ln 2} \cdot \ln\left\{ \frac{\sqrt{1+16\cdot 2^q} - 1}{8} \right\} \right) \tag{73}$$

$$\alpha(q) = 2 + \frac{8 \cdot 2^{-q}}{\sqrt{1+16\cdot 2^{-q}} - 1 - 16 \cdot 2^{-q}} \tag{74}$$

and

$$f(\alpha(q)) = \frac{8q \cdot 2^{-q}}{\sqrt{1+16\cdot 2^{-q}} - 1 - 16 \cdot 2^{-q}} - \frac{1}{\ln 2} \ln\left\{ \frac{\sqrt{1+16\cdot 2^{-q}} - 1}{8} \right\} \tag{75}$$

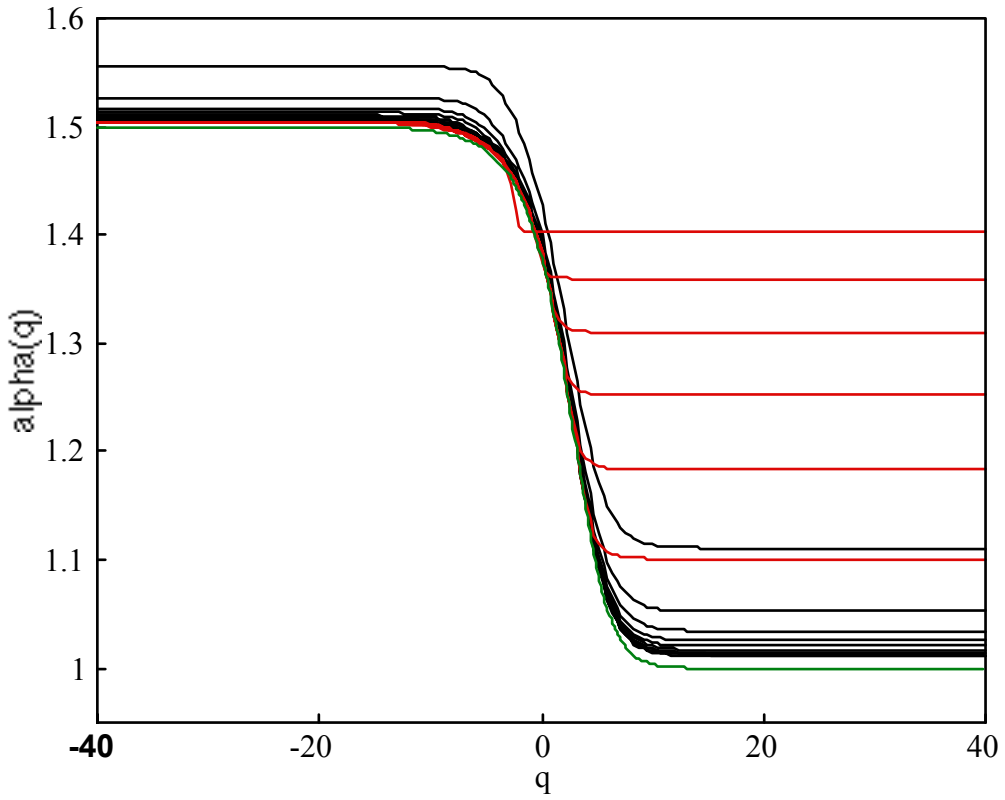

Figure 22. This is the function α(q) for the even family. The black curves are solutions for boxes larger than the largest particle, the red curves are solutions for boxes smaller than the largest particle and the green is the exact solution.

In Fig. 21 and 22 we show the function *α(q)* for the odd and the even family respectively. As we can see, smaller box-sizes give the best result for

negative *q*-values and large box-sizes give solutions which converge fast for positive *q*:s.

Figure 23 and 24 shows the function *f(q)* for the odd and the even family respectively. As for *α(q)*, the smaller box-sizes give the best result for negative *q*-values and large box-sizes give solutions which converge fast for positive *q*:s

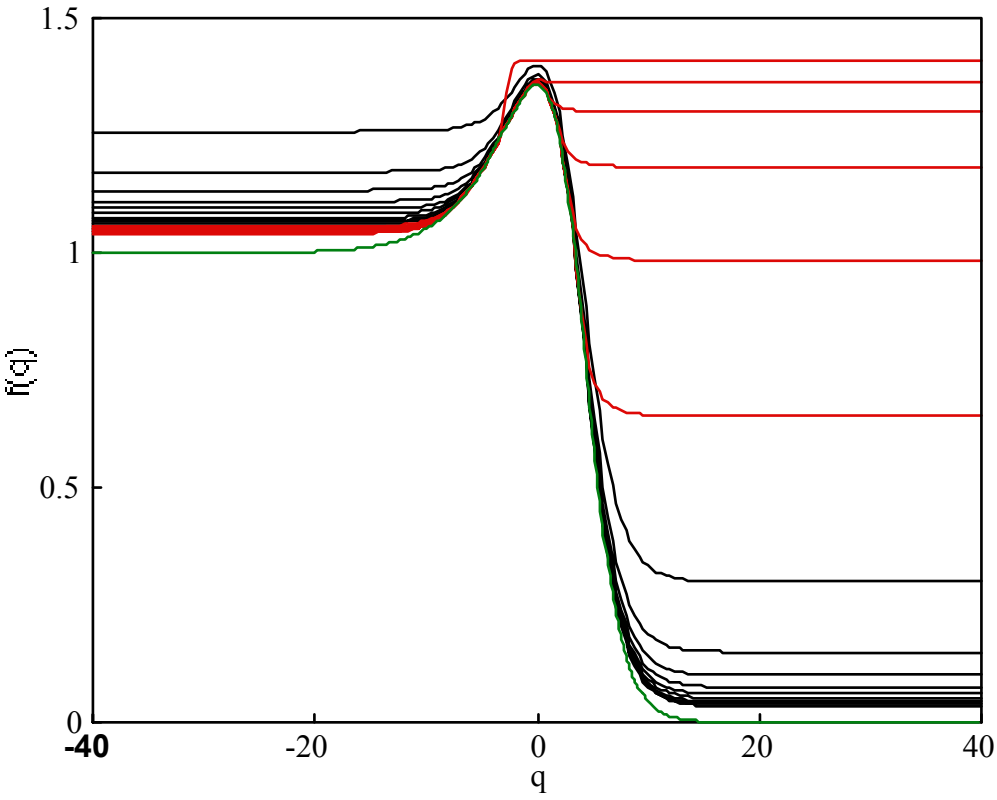

Figure 23. This is the function f(q) for the even family. The black curves are solutions for boxes larger than the largest particle, the red curves are solutions for boxes smaller than the largest particle and the green is the exact solution.

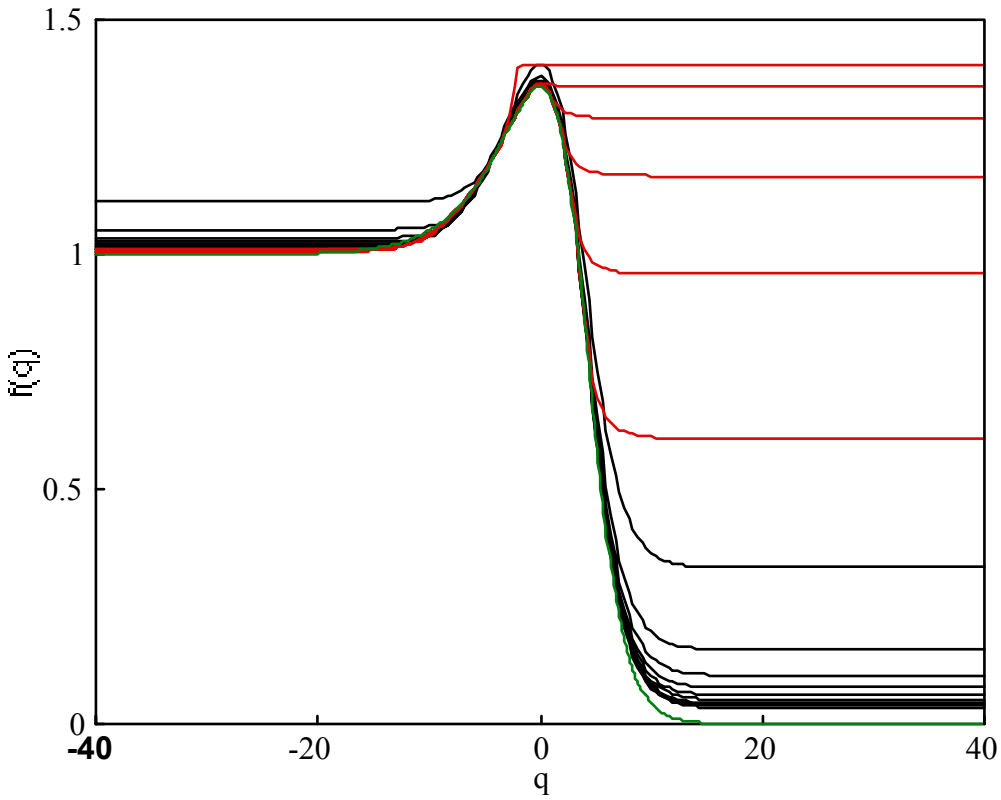

Figure 24. This is the function f(q) for the even family. The black curves are solutions for boxes larger than the largest particle, the red curves are solutions for boxes smaller than the largest particle and the green is the exact solution.

If we plot $f(q)$ versus $\alpha(q)$ we get the $f(\alpha)$-spectrum, Fig. 25 and Fig. 26. Figure 25 show the odd family and Figure 26 the even family. Compare this figures with those in paper II. The solutions in paper II are calculated from the fractal level $n = 16$, i.e., $4^{16} \approx 4.3 \cdot 10^9$ particles and the solutions below from level $n = 90$.

We observe that the red curves, i.e., solutions for box-sizes smaller than the largest particles are closer to the exact solution at the right side of the $f(\alpha)$-spectrum. This side correspond to negative values of the momentum q. The left part of the $f(\alpha)$-spectrum, i.e., for positive q-values, boxes of sizes larger than the largest particle, that in the middle of the snowflake, lies closer to the exact solution, the green curve.

This observation is important in the calculation of the $f(\alpha)$-spectrum. To get a good result in such a calculation it is important to vary the sizes of the boxes and then select the left-most value of α for each f both on the right- and the left part of the $f(\alpha)$-spectrum.

We also observe that for the odd family all curves ends up at the exact value of α, i.e., $\alpha = 1.5$. The $f(\alpha)$-spectrum start at the point $(1, 0)$ and ends up in the point $(1.5, 1)$. We can understand this since the first point correspond to the limit where $q \to \infty$. This limit is dominated by the largest particles in the fractal, since that part gives the largest probability see Eq. (17). Since we only have one particle with the largest size the value of $f \to 0$. The value of α is also given since the largest particle consist of 4^n particles of size 4^{-n} at each level, and $\alpha \to ln(4^n)/ln(1/4^{-n}) = 1$.

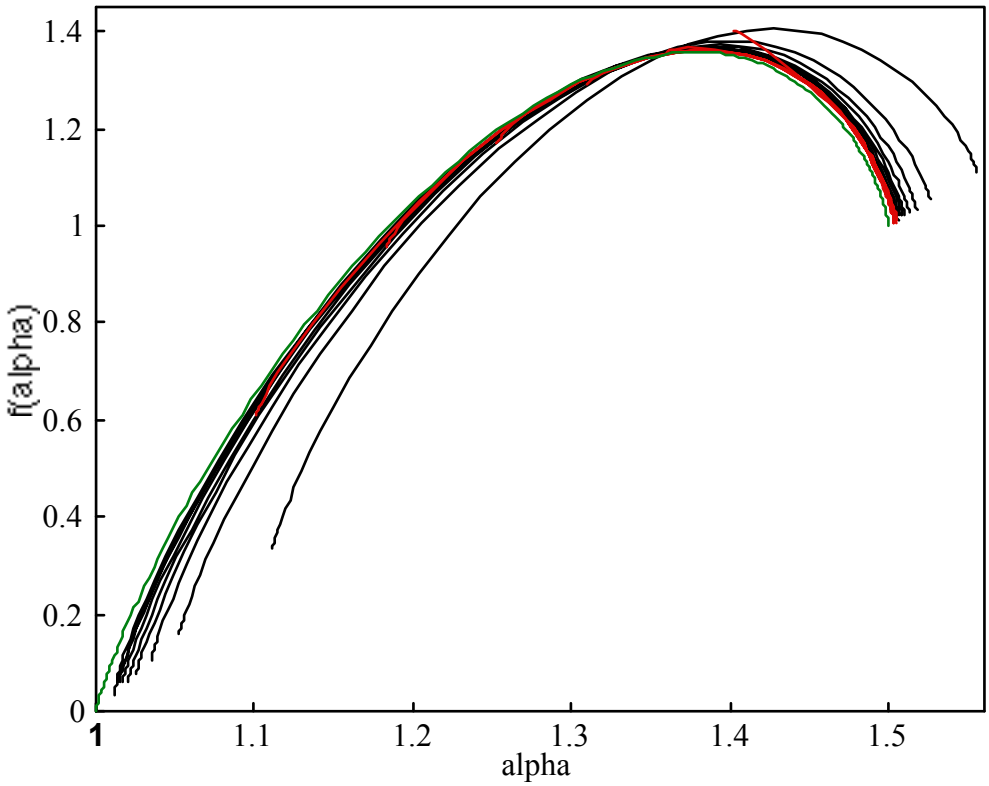

Figure 25. This is the $f(\alpha)$-spectrum for the even family. The black curves are solutions for boxes larger than the largest particle, the red curves are solutions for boxes smaller than the largest particle and the green is the exact solution.

Similarly we can understand the values at the end point of the $f(\alpha)$-spectrum since this is dominates by the smallest particles when $q \to -\infty$. At this point we have 4^n particles of size 4^{-n}, i.e., $f \to ln(4^n)/ln(1/4^{-n}) = 1$ and the fractal consists of 8^n particles of size 4^{-n} hence $\alpha \to ln(8^n)/ln(1/4^{-n}) = ln(8)/ln(4) = 1.5$.

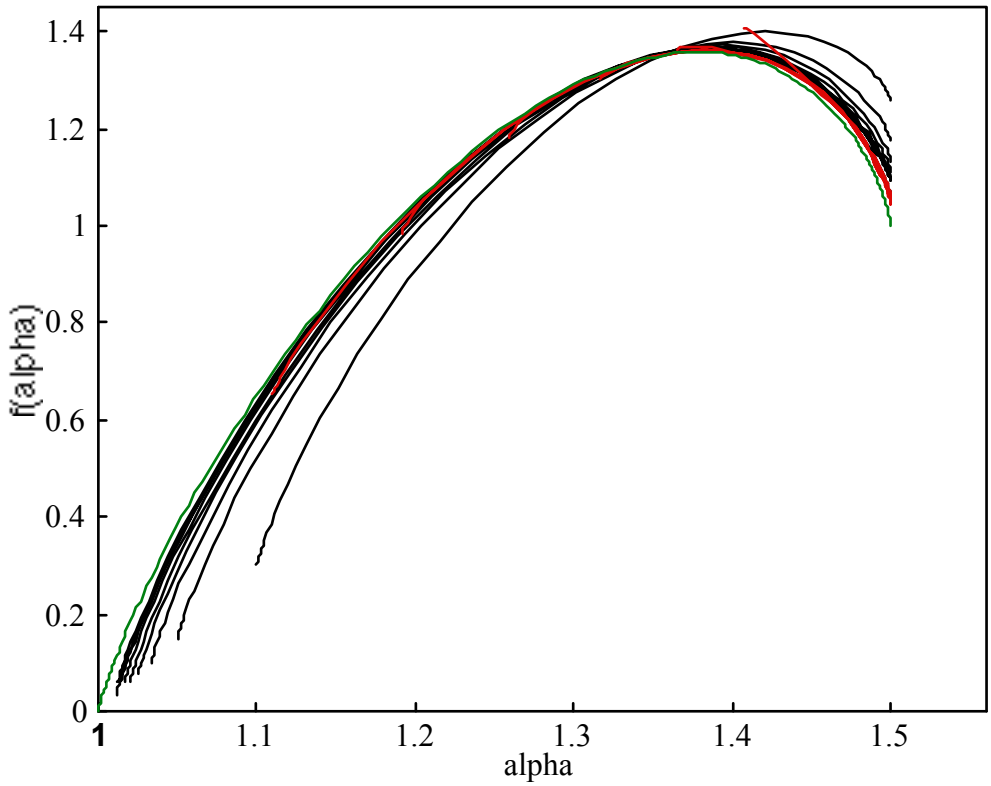

Figure 26. This is the f(α)-spectrum for the odd family. The black curves are solutions for boxes larger than the largest particle, the red curves are solutions for boxes smaller than the largest particle and the green is the exact solution.

In Fig. 27 and Fig. 28 we show the generalized dimensions $D_q(q)$ for the even and odd family respectively. As we can see, smaller boxes is best for negative values of q and larger boxes for positive q:s. By varying the box-size and select the smallest value of D_q for each value of q, we can extract the closest solution to the exact curve.

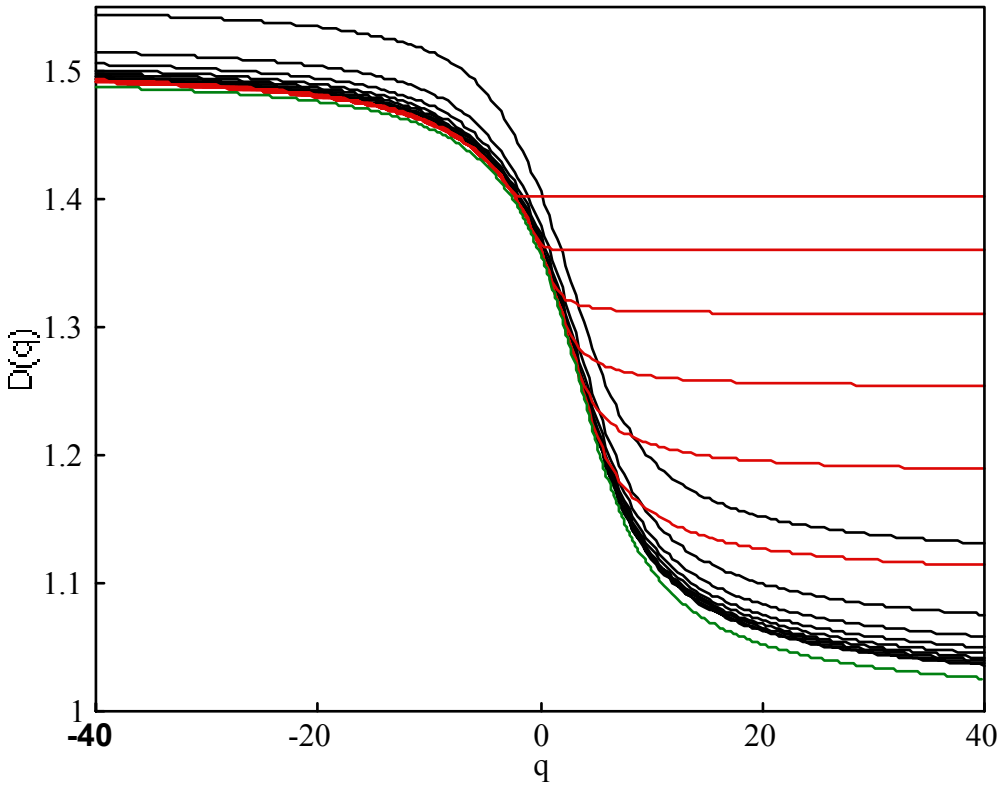

Figure 27. This is the Generalized dimensions D_q for the even family. The black curves are solutions for boxes larger than the largest particle, the red curves are solutions for boxes smaller than the largest particle and the green is the exact solution.

We also observe that the odd family converge fastest, special for negative values of the momentum q. This is due to the fact that this family have a large number of boxes containing reduced copies of the whole snowflake fractal.

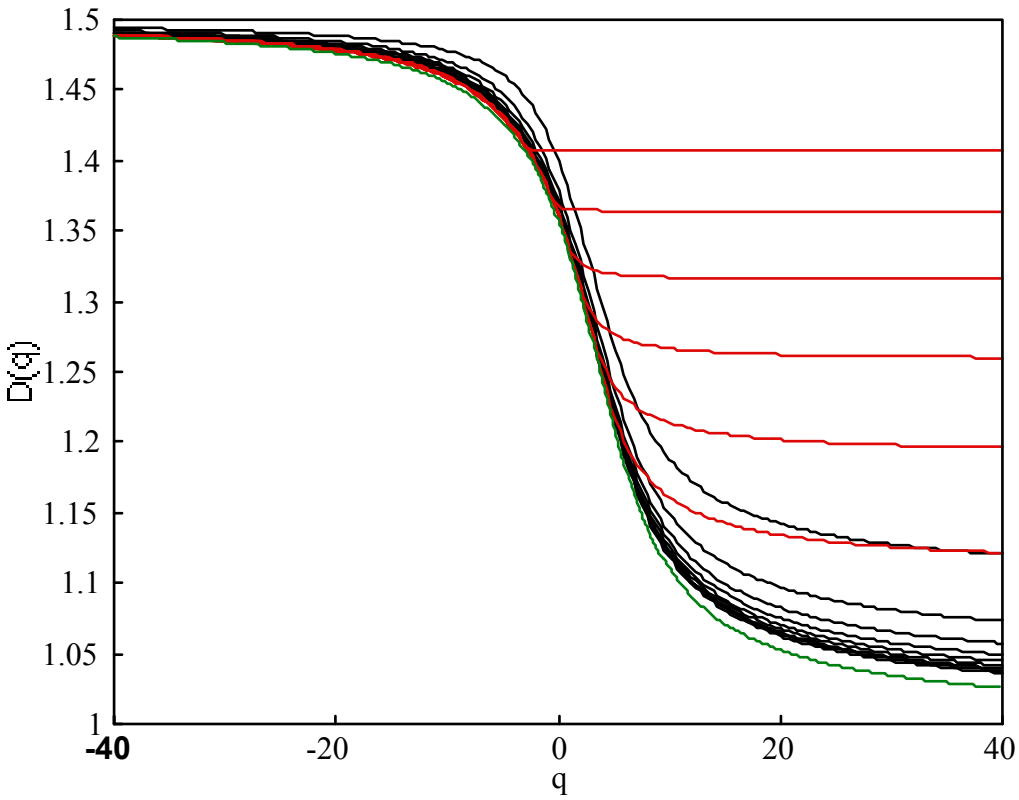

Figure 28. This is the Generalized dimensions D_q for the odd family. The black curves are solutions for boxes larger than the largest particle, the red curves are solutions for boxes smaller than the largest particle and the green is the exact solution.

3.7: Box-counting on a gas evaporated metal particle aggregate

One goal in the calculations of fractal dimensions of aggregates, is to compare with the dimensions given by different computer aggregation models. Such models have been proven to be useful, in order to understand the processes that give rise to fractal structures.

3.7.1: Diffusion Limited Aggregations

One common computer model is DLA, Diffusion Limited Aggregation. This model has been found to be relevant to a large variety of processes including fluid-fluid displacement in porous media, dielectric breakdown, electrodeposition and possibly growth processes. The DLA model illustrates that simple growth and aggregation models could lead to valuable insights into important physical and chemical processes.

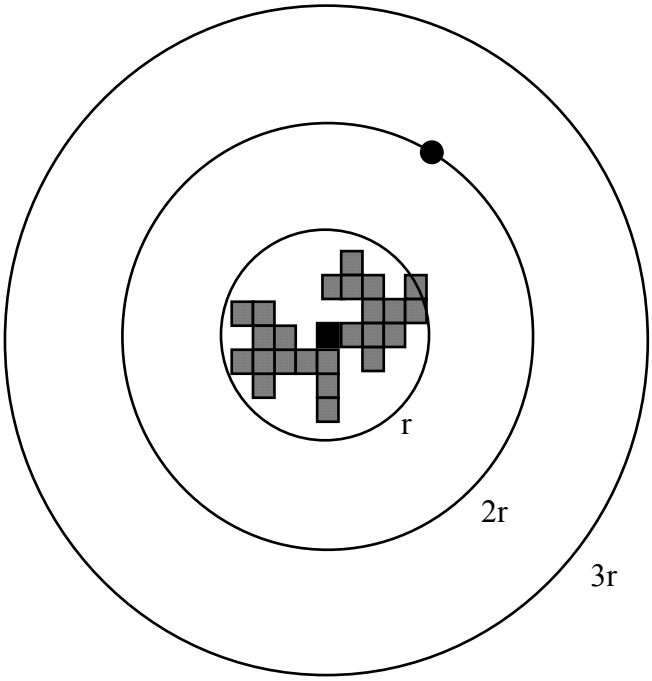

Figure 29. The DLA model in two dimensions. Start with a single occupied site (the centre). Place a single particle at a random position on a circle outside the cluster and use random walk on a lattice. If the particle hits the cluster it grows with the lattice size, if it walks outside the outer circle, take a new particle on the starting circle.

In a DLA model we place a particle from a randomly selected point on a circle outside the cluster. This particle can move on a lattice with random walk. If the particle hits the cluster it stops and the cluster grows with one cell. On the other hand, if the particle moves outside an outer circle, we place a new particle at a randomly selected point on the starting circle. The simulation starts with a single occupied site, the black one in the middle.

This simple two-dimensional model can be modified (generalized) in different ways. A common generalisation is to introduce a sticking probability $S \leq 1$. The Hausdorff dimension given by the DLA model in two dimensions is $D_0 = 1.70 \pm 0.06$ for $S = 1$ and $D_0 = 1.72 \pm 0.06$ for $S = 0.25$ [20].

3.7.2: Ballistic Aggregations

This model was one of the first cluster aggregations models, developed by M. J. Vold, more than 25 years ago [20]. In contrast to DLA, with a small mean free path compared with the size of the aggregate, the mean free path of the ballistic models is large. We begin with a single stationary particle, and one free particle in a random ballistic (linear) trajectory in the vicinity of the

stationary particle. If the ballistic particle hits the stationary it sticks to that point and a stationary cluster is formed. Then we add new ballistic particles, one at a time, until a large cluster has formed.

A ballistic aggregate becomes very dense and the fractal dimension is very close to the Euclidean dimension of the embedding space. For large clusters, up to 250 000 particles, the Hausdorff dimension is larger than 1.95 in two, and larger than 2.3 in three dimensional simulations[20].

3.7.3: Cluster-Cluster Aggregations

In this models we consider a squared lattice, L by L with L^2 sites. We place N particles at random positions on the lattice and let them move randomly. On collisions they stick, and form larger and larger clusters that can collide with other cluster. In the final state we have one large cluster. There are many extensions to cluster-cluster aggregations, the cluster can rotate and the lattice can be multidimensional etc. Three common versions of cluster-cluster aggregation is DLCA, Diffusion-Limited Cluster-Cluster Aggregation where the cluster moves with random walk, Ballistic cluster-cluster aggregation where each cluster moves along ballistic (linear) trajectories and the chemical cluster-cluster aggregation. The last model is the same as the ballistic but with vanishing sticking probability. In this limit, the clusters have time to investigate all the possible sticking situations before choosing one. This model is used to study colloids, where we have a strong repulsive barrier that the particles must overcome before being attracted by the short range Van der Waals forces. The theoretical results of cluster-cluster dimension is 1.44 and 1.78 in a two and three dimensional simulation respectively. If ballistic trajectories are used the dimensions are 1.55 and 1.91 and in a cluster-cluster chemical simulation the result is 1.55 and 2.04 [20].

3.7.4: Aggregate of magnetic particles

In paper III we study a fractal aggregate of magnetic cobalt particles. The aggregate were produced by inert-gas evaporation[21] from a heated tungsten spiral in a conventional bell-jar system. The evaporation took place in 1.3 kPa of argon gas and resulted in particles of about 100 Å radius that were clustered into large connected aggregate as seen in Fig. 30. Particles interacting via long-range forces produce aggregate with quite different scaling properties [22]. We estimated the Hausdorff dimension of the fractal to be 1.703 ± 0.006.

Figure 30. A fractal aggregate of gas-evaporated magnetic cobalt particles..

REFERENCES:

[1] W. F. Ganong, Review of Medical Physiology, Sth Ed. Lange Medical Publications, California 1977.

[2] Peitgen, H. O., and Richter, Peter, The Beauty of Fractals (1986).

[3] B. B. Mandelbrot, Les Object Fractals, Flammarion, Paris 1975. - B. B. Mandelbrot, Fractals: Form, Chance and Dimensions, Freeman, San Fransisco 1977. B. B. Mandelbrot The Fractal Geometry of Nature, Freeman, San Fransisco 1982.

[4] F. Hausdorff, Dimension und äußeres Maß, Mathematische Annalen 79, 157 (1919).

[5] Fleischmann, M., and Teldesley, D.J., eds., Fractals in the Natural Sciences (1990);

[6] Hideki, Takayasu, Fractals in the Physical Sciences (1990);

[7] Gleick, James, Chaos: Making a New Science (1987);

[8] J.-P. Eckmenn and D. Ruelle, "Ergodic Theory of Chaos and Strange Attractors," Rev. Mod. Phys. 57, 617 (1985)

[9] J. Guckenheimer and P. Holmes, "Nonlinear Oscillations, Dynamical Systems, and Bifurcations of Vector Fields", Appl. Math. Sci. 42, Springer, New York (1983).

[10] K. J. Falconer, The Geometry of Fractal Sets. Cambridg University Press. Cambridge 1985.

[11] L. Pietronero and E. Tosatti (eds.), Fractals in Physics. North-Holland, Amsterdam 1986.

[12] J. Feder, Fractals, Plenum Press, New York 1988.

[13] T. C. Halsey, M. H. Jensen, L. P. Kadanoff, I. Procaccia and B. I. Shraiman, Phys. Rev. A 33, 1141 (1986).

[14] H. G. E. Hentschel and I. Procaccia, Physica D 8, 435 (1983).

[15] B. B. Mandelbrot, J. Fluid. Mech. 62, 331 (1974).

[16] P. Grassberger, Phys. Lett. 97 A, 227 (1983); 107 A, 101 (1985).

[17] A. Renyi, Probability Theory, North Holland, Amsterdam (1970)

[18] C. Amitrano, A. Coniglio, F. dj Liberto, Phys. Rev. Lett. 57 1016 (1986). - Y. Hayakawa, S. Sato, M. Matsushita, Phys. Rev. A 36 1963 (1987).

[19] J. D. Farmer, Z. Naturforsch. 37 a, 1304 (1982).

[20] P. Meakin, Computer Simulations of growth and aggregation processes in On Growth and Form (edited by H. E. Stanley and N. Ostrowsky) 1986, Martinus Nijhoff Publishers, Dordrecht.

[21] C. G. Granqvist, R. A. Buhrman. J. Appl. Phys. 47, 2200 (1976)

[22] G. Helsen, A. T. Skjeltorm, P. M. Mors, R. Boet and R. Jullien, Phys. Rev. Lett. 61, 1736 (1988).

INDEX: